Phase transitions in a two-dimensional lattice gas model of orientable diatomic molecules

W. Rżysko* and A. Patrykiejew
Faculty of Chemistry, MCS University, 20031 Lublin, Poland

K. Binder
Institut für Physik, Johannes Gutenberg-Universität, 55099 Mainz, Germany
(Received 28 April 2005; revised manuscript received 1 August 2005; published 17 October 2005)

Using a lattice-gas version of the extended Blume-Emery-Griffiths spin-1 model and Monte Carlo simulation methods, the ordering of heteronuclear diatomic molecules (*AB*) adsorbed on a corrugated crystal surface with adsorption sites forming a square lattice is studied. The applied lattice model assumes that the adsorbed molecules are all vertically oriented with respect to the surface and takes into account the interaction between the first- as well as between the second-nearest neighbors. First, assuming that all interactions in the system are nonrepulsive, the order-disorder transitions for different possible phases are discussed. In particular, it is demonstrated that the critical exponents of the order-disorder transitions for the two ordered phases (*SAF* and A_3B) are nonuniversal and change with the model parameters. Then, assuming that the first-nearest neighbor interactions are nonattractive, the evolution of the phase diagram topology with the change of the model parameters is evaluated. The critical exponents associated with the continuous phase transitions have been estimated using the finite size scaling analysis. It is demonstrated that the nature of the order-disorder phase transitions depends on the structure of the ordered states and that they belong to different classes of universality. It is also found that the phase diagrams exhibit the presence of critical, tricritical, and critical end points, depending on the magnitudes of coupling constants.

DOI: 10.1103/PhysRevB.72.165416 PACS number(s): 64.60.Cn, 68.35.Rh, 68.43.−h

I. INTRODUCTION

The adsorbed layers formed by linear molecules on well-defined crystalline surfaces are known to form a variety of ordered phases with a structure depending on the orientation of the adsorbed molecules with respect to the surface and to each other.[1–6] One of the simplest possible situations involves monolayer adsorption of asymmetric diatomic molecules (*AB*) on a square lattice of sites. Well-known examples of such systems are the monolayers of CO on NaCl(100) or MgO(100) surfaces.[7–9] Among the characteristic features of the above-mentioned systems is a strong dependence of the surface binding energy on the orientation of an adsorbate molecule. This leads to the formation of films in which, unlike in the case of adsorption of homonuclear diatomics,[1,2,4,5] the adsorbed molecules are predominantly bound to the surface by one end (*A* or *B* atom), and the monolayer is tilted with respect to the surface. For example, Monte Carlo simulations for a CO monolayer on NaCl(100) surface[7] demonstrated the formation of the $p(2\times1)$ structure with a glide plane and with the carbon atoms down, and pointing towards Na^+ ions, and the tilt angle of about 24° at low temperatures. The results of Monte Carlo calculations were found to be consistent with experimental data[10,11] and with theoretical calculations.[12,13]

A simple theoretical model that involves the effects due to orientation-dependent admolecule-admolecule as well as admolecule-surface interactions is the spin-1 lattice model,[14–16] in which the adsorbate molecules are oriented vertically to the surface in one of the two possible orientations, with the *A* end down or with the *B* end down. In general, these two possible orientations have different binding energies to the surface. Moreover, the interaction energy between a pair of the adsorbed molecules is also orientation dependent and, in the simplest version, depend only on the relative orientation of the molecules adsorbed at adjacent sites. Thus, one neglects any effects due to surface-mediated interactions.[17]

Several versions of the spin-1 lattice model have been considered and applied to a large number of problems in the condensed-matter physics, including the description of simple and multicomponent fluids,[14,16,18] dipolar and quadrupolar orderings in magnets,[19,20] ordering in semiconducting alloys,[21] microemulsions,[22] and adsorbed layers.[4,5,23–25] Spin-1 lattice models have been studied by a variety of theoretical methods: mean-field,[16,18,25–27] cluster variation method,[28–30] transfer matrix finite size scaling,[31,32] high-temperature series expansion,[33] renormalization group method,[34,35] and Monte Carlo simulations.[36–39] The interest in spin-1 models is highly stimulated by the richness of their phase diagrams, arising from the competing interactions. In the most general case, one needs to take into account the bilinear, biquadratic, as well as quadrilinear interactions between nearest neighbors as well as linear and quadratic single spin terms, which represent the contributions coming from the single spin anisotropy and the external field, respectively. Although the hitherto studied versions of spin-1 models have usually involved only the first-nearest neighbor interactions, several different phase diagram topologies have been found.[16,18,30,40] A rather simple Blume-Capel (BC) model has been found to possess the tricritical point in the phase diagram.[22,33,41–46] The transfer matrix finite size scaling calculations of Badehdah *et al.*[33] suggested that the inclusion of the longer-range (second-nearest neighbor) interactions to the BC model may violate the ordinary

universality hypothesis, when the interaction parameters are suitably chosen. The Blume-Emery-Griffiths (BEG) model with negative biquadratic interaction[47,48] was found to exhibit a very rich phase behavior, which involves ferrimagnetic and antiquadrupolar phases and multicritical points of higher order.

In this paper we present a lattice gas version of the model, which involves the interaction between the first- as well as between the second-nearest neighbors. Using Monte Carlo methods we investigate the structure and properties of different possible ordered phases. The order-disorder phase transitions and phase diagrams for a series of systems characterized by different interaction parameters are discussed.

The paper is organized as follows. In Section II we present the model and discuss its ground state properties. Then, Sec. III summarizes the description of Monte Carlo methods used here and the methodology applied. The results of our calculations are presented and discussed in Secs. IV and V. Section IV is primarily devoted to the discussion of the order-disorder phase transitions in a series of systems with nonrepulsive first- as well as the second-nearest neighbor interactions. Then, in Sec. V we discuss the phase behavior of the systems with the nonattractive first-nearest neighbor interactions. In particular, we shall elucidate the changes in the phase diagram topology resulting from the variation of the model parameters, which define the interaction energies between the pairs of the first- and the second-nearest neighbors of the same and opposite orientation. The paper is concluded by Sec. VI, where we summarize our findings.

II. THE MODEL

As it has been already mentioned in the Introduction, we consider a monolayer adsorption of diatomic heteronuclear molecules AB on a square lattice of sites. Each adsorbed molecule is assumed to take on the vertical orientation with respect to the surface plane and can be bound to the surface via either atom A or B, so that the energy of adsorption depends on the orientation of the adsorbed molecule. To the molecule adsorbed at the site i we assign a variable s_i, which is equal to 1 (-1) when the molecule is bound to the surface via atom $A(B)$. Thus, the surface potential is a function of the variable s_i and can be represented as

$$V(s_i) = \begin{cases} V_A, & s_i = 1, \\ V_B, & s_i = -1. \end{cases} \tag{1}$$

Then, we assume that a pair of molecules interacts one with another, whenever they occupy the first- or the second-nearest neighboring sites. The energy of interaction between such a pair also depends on the relative orientation of interacting molecules and can be written as $u_k(s_i, s_j)$, where $k = 1$ or 2 for the first- and the second-nearest neighbor interaction, respectively, while s_i and s_j are the above-defined spin variables, which represent the orientation of each molecule. Here we assume that the interaction energy depends only on the relative orientation of both molecules, so that we can define $u_k(s_i, s_j)$ as

$$u_k(s_i, s_j) = \begin{cases} u_{k,a}, & s_i = s_j, \\ u_{k,b}, & s_i \neq s_j, \end{cases} \quad k = 1,2 \tag{2}$$

With the above assumptions, the Hamiltonian of the model reads

$$\mathcal{H} = \frac{1}{2}\sum_{\langle ij\rangle_1} n_i n_j u_1(s_i, s_j) + \frac{1}{2}\sum_{\langle ij\rangle_2} n_i n_j u_2(s_i, s_j) + \sum_i V(s_i) n_i - \mu \sum_i n_i, \tag{3}$$

where n_i is the occupation variable, equal to 0 (1) when the site i is empty (occupied), the first (second) sum runs over all pairs of the first- (second) nearest neighbors, μ is the chemical potential, and the sums in the third and fourth terms run over all sites. Here we assume that all energies $[u_k(s_i, s_j)$ and $V(s_i)]$ are negative (positive) for attractive (repulsive) interactions.

By assigning to each lattice site the spin variable $S_i = \pm 1, 0$, and replacing the occupation variable n_i by S_i^2, the above lattice-gas model Hamiltonian can be mapped onto the appropriate spin-1 lattice model Hamiltonian

$$\mathcal{H}' = \frac{1}{2}\bar{u}_1 \sum_{\langle ij\rangle_1} S_i^2 S_j^2 + \frac{1}{2}\Delta\hat{u}_1 \sum_{\langle ij\rangle_1} S_i S_j + \frac{1}{2}\bar{u}_2 \sum_{\langle ij\rangle_2} S_i^2 S_j^2 + \frac{1}{2}\Delta\hat{u}_2 \sum_{\langle ij\rangle_2} S_i S_j + \bar{V}\sum_i S_i^2 - \Delta\hat{V}\sum_i S_i - H\sum_i S_i^2 \tag{4}$$

where

$$\bar{u}_k = \tfrac{1}{2}(u_{k,a} + u_{k,b}), \quad \Delta\hat{u}_k = \tfrac{1}{2}(u_{k,a} - u_{k,b}), \tag{5}$$

$$\bar{V} = \tfrac{1}{2}(V_A + V_B), \quad \Delta\hat{V} = \tfrac{1}{2}(V_B - V_A), \tag{6}$$

and H is the external field, which can be related to the chemical potential μ.

Without losing generality we can assume that $V_A < V_B$, i.e., a single molecule is preferentially adsorbed via the atom A. Then, it is convenient to define the parameters $\Delta V = V_B - V_A = 2\Delta\hat{V}$, $\Delta u_1 = u_{1,a} - u_{1,b} = 2\Delta\hat{u}_1$, and $\Delta u_2 = u_{2,a} - u_{2,b} = 2\Delta\hat{u}_2$, since the structure of different possible ordered phases discussed below depends only on the above-specified differences between interaction energies.

In the ground state, i.e., at the temperature $T = 0$, one can readily calculate the grand potential density for any ordered phase α, ω_α, directly from the Hamiltonian, since each ordered phase α is characterized by specific symmetry properties which determine the arrangement of differently oriented molecules over the surface, i.e., a set of variables $\{n_i, s_i\}$ $(i = 1, 2, \ldots)$.

Then we define the densities of differently oriented molecules in the phase α

$$\rho_{\alpha,l} = L^{-2}\sum_i n_i \delta_{s_i,l}, \quad \text{where } l = 1 \text{ or } -1, \tag{7}$$

where L^2 is the number of sites, and the total density of the adsorbed layer $\rho_\alpha = \rho_{\alpha,1} + \rho_{\alpha,-1}$.

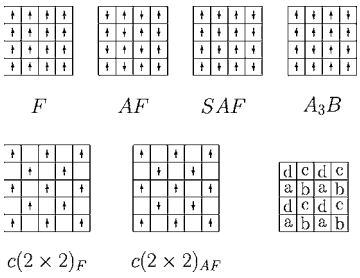

FIG. 1. Schematic representation of different possible ordered states (↑ and ↓ denotes molecules adsorbed via the atom A and B, respectively) and the decomposition of a square lattice into four equivalent sublattices a, b, c, and d.

Here, we assume that the first-nearest neighbor interactions $u_{1,k}(k=a,b)$ can be either attractive or repulsive while the second-nearest neighbor interactions $u_{2,k},(k=a,b)$ are nonrepulsive. Under such conditions, the model predicts that when the first-nearest neighbor interactions are nonrepulsive all the possible ordered states have the total density $\rho_\alpha=1$, i.e., all sites are occupied, and the following ordered phases can appear: F, AF, SAF and A_3B, which are schematically shown in the upper part of Fig. 1. On the other hand, when the first-nearest neighbor interactions ($u_{1,a}$ and/or $u_{1,b}$) become repulsive, the two additional ordered states of the lower density ($\rho_\alpha=0.5$), labelled as $c(2\times2)_F$ and $c(2\times2)_{AF}$, can also be formed (see Fig. 1). Of course, one has also to take into account the gas phase (g), which at the ground state has the density equal to zero. Table I summarizes the densities $\rho_{\alpha,l}$ and the grand canonical potential densities (ω_α) for all the phases mentioned above.

Throughout this paper we assume that $V_A=-2.0$ and $V_B=-1.0$, so that $\Delta V=1.0$. We also take $|V_B|$ as the unit of energy, so that the interaction energies, $u_{k,l}$ ($k=1$, 2 and $l=a,b$), the differences $\Delta u_k(k=1,2)$ and ΔV, as well as all other energy-like quantities, such as temperature and the chemical potential, are expressed in units of $|V_B|$.

When the first-nearest neighbor interactions are nonrepulsive only the ordered states F, AF, SAF, and A_3B can appear, and the ground state phase diagram for such systems is depicted in Fig. 2. The locations of the three triple points t_1, t_2, and t_3 are entirely determined by the values of Δu_1, Δu_2, and ΔV:

$$t_1:\Delta u_1=0.25\Delta V,\quad \Delta u_2=0.0,$$

TABLE I. The fractional densities $\rho_{\alpha,l}$ and the grand canonical potential densities ω_α for the different phases α at $T=0$.

α	$\rho_{\alpha,1}$	$\rho_{\alpha,-1}$	ω_α
g	0.0	0.0	0.0
F	1.0	0.0	$2u_{1,1}+2u_{2,1}+V_A-\mu$
AF	0.5	0.5	$2u_{1,2}+2u_{2,1}+0.5(V_A+V_B)-\mu$
SAF	0.5	0.5	$u_{1,1}+u_{1,2}+2u_{2,2}+0.5(V_A+V_B)-\mu$
A_3B	0.75	0.25	$u_{1,1}+u_{1,2}+u_{2,1}+u_{2,2}+0.75V_A+0.25V_B-\mu$
$c(2\times2)_F$	0.5	0.0	$u_{2,1}+0.5V_A-0.5\mu$
$c(2\times2)_{AF}$	0.25	0.25	$u_{2,2}+0.25(V_A+V_B)-0.5\mu$

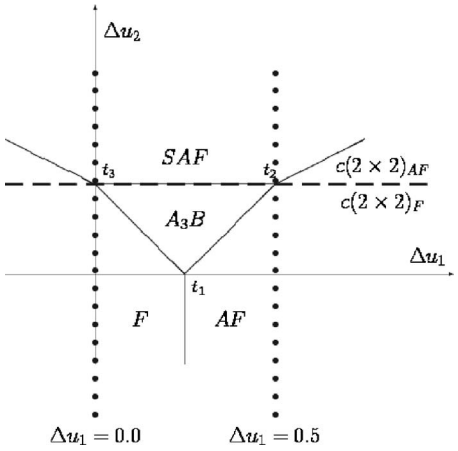

FIG. 2. Ground state phase diagram for the model. The thin solid lines delimit the regions of stability of the ordered structures of the density $\rho=1.0$, while the horizontal thick dashed line delimits the regions of stability of the phases $c(2\times2)_F$ and $c(2\times2)_{AF}$. The vertical dotted lines mark the paths along which the calculations have been performed.

$$t_2:\Delta u_1=0.5\Delta V,\quad \Delta u_2=0.25\Delta V,$$

$$t_3:\Delta u_1=0.0,\quad \Delta u_2=0.25\Delta V. \tag{8}$$

Moreover, using the data from Table I it can be readily shown that the necessary condition for the appearance of the low density phases $c(2\times2)_F$ and $c(2\times2)_{AF}$ is that $u_{1,a}>0$. Which of these two phases does exist depends on the values of the parameters Δu_2 and ΔV. The phase $c(2\times2)_F$ is stable when $\Delta u_2<0.25\Delta V$, while the phase $c(2\times2)_{AF}$ is stable when $\Delta u_2>0.25\Delta V$. The phase boundary between these two ordered phases is marked by a thick horizontal dashed line in Fig. 2, located at $\Delta u_2=0.25\Delta V$.

III. MONTE CARLO METHOD AND METHODOLOGY

The model presented above has been studied by Monte Carlo methods in the grand canonical as well as in the canonical ensembles,[49,50] using the simulation cell of the size $(L\times L)$, with L ranging between 12 and 160, and periodic boundary conditions.

In order to gain information about the structure of different ordered states a set of suitably defined order parameters have been used. The total density as well as the densities of differently oriented particles allow us to distinguish between the phases F, AF, and A_3B as well as between both the $c(2\times2)_F$ and $c(2\times2)_{AF}$ phases of lower density, but do not provide information sufficient to tell which of the phases AF or SAF is present (see Table I). Therefore, it is more convenient to define the order parameters in terms of sublattice magnetizations using the spin-1 model Hamiltonian (4) rather than the lattice-gas model Hamiltonian (3).

If one decomposes the entire lattice into four interpenetrating and fully equivalent sublattices, as shown in Fig. 1, the average magnetization of each sublattice k (a, b, c, and d) is given by

TABLE II. The values of the order parameters in the ordered phases predicted by the present model.

	F	AF	SAF	A_3B	$c(2\times2)_F$	$c(2\times2)_{AF}$
$\lvert\Psi_{SAF}\rvert$	0.0	0.0	1.0	0.5	0.0	0.5
$\lvert\Psi_3\rvert$	0.0	1.0	0.0	0.5	0.5	0.0
$\lvert\Psi_4\rvert$	1.0	0.0	0.0	0.5	0.5	0.0

$$m_k = \frac{1}{L^2}\sum_{i\in k} S_i. \tag{9}$$

Using the above-defined magnetizations we define the following four order parameters:

$$\Psi_1 = m_a - m_b - m_c + m_d, \tag{10}$$

$$\Psi_2 = m_a + m_b - m_c - m_d, \tag{11}$$

$$\Psi_3 = m_a - m_b + m_c - m_d, \tag{12}$$

$$\Psi_4 = m_a + m_b + m_c + m_d. \tag{13}$$

The order parameters Ψ_1 and Ψ_2 represent two components of the order parameter suitable to detect the presence of the phases SAF and $c(2\times2)_{AF}$. In the case of a square lattice considered here, the two components of the above order parameter are equivalent and the order parameter is invariant under global rotation. Then it is the magnitude of the order parameter which matters, and we define the order parameter Ψ_{SAF} as

$$\Psi_{SAF} = \sqrt{\Psi_1^2 + \Psi_2^2}. \tag{14}$$

In the case of a perfect SAF phase $\Psi_{SAF}=1.0$, while in the case of $c(2\times2)_{AF}$, $\Psi_{SAF}=0.5$. The order parameter Ψ_3 assumes nonzero values for the structures $c(2\times2)_F$, in which it equals to ±0.5, and $AF(\Psi_3=\pm1.0)$, while the order parameter Ψ_4 assumes the value of 1.0, when the system orders into the phase F and 0.5 when the low density phase $c(2\times2)_F$ occurs.

In practice the order parameters defined above, Ψ_{SAF}, Ψ_3, and Ψ_4, suffice to distinguish all ordered phases predicted by the model (see Table II). In the case of a fully occupied lattice, it is also convenient to define two other order parameters, which are useful for detecting the phases SAF and A_3B. Namely, by dividing the lattice into cells, each containing four sites belonging to different sublattices, the order parameter suitable for detecting the phase SAF can be defined as[51]

$$\Psi_5 = \sum_n (S_{n,a} - S_{n,c})(S_{n,b} - S_{n,d}), \tag{15}$$

where the sum runs over all cells and $S_{n,k}$ represent the spin variable of the site belonging to the cell n and the sublattice k ($k=a,b,c$, or d). The order parameter Ψ_5 is equal to zero in all phases but SAF, for which it is equal to unity. In the case of the ordered phase A_3B one can define the order parameter which has two mutually orthogonal components

$$\Psi_{6,1} = \sum_n (S_{n,a} - S_{n,c})(S_{n,b} + S_{n,d}) \text{ and}$$

$$\Psi_{6,2} = \sum_n (S_{n,a} + S_{n,c})(S_{n,b} - S_{n,d}) \tag{16}$$

of the length

$$\Psi_6 = \sqrt{\Psi_{6,1}^2 + \Psi_{6,2}^2}, \tag{17}$$

which is nonzero, and equal to unity, only when the system orders into a perfect A_3B phase.

The above-defined order parameters are complemented by the corresponding susceptibilities

$$\chi_{\Psi,L} = \frac{1}{kT}[\langle\Psi^2\rangle - \langle|\Psi|\rangle^2] \tag{18}$$

and the fourth-order cumulants[50,52]

$$U_{\Psi,L} = 1 - \frac{\langle\Psi^4\rangle}{3\langle\Psi^2\rangle^2}. \tag{19}$$

In the above, Ψ denotes any of the above-defined order parameters.

Apart from the above-defined structural parameters we have also calculated the average density,

$$\rho = \frac{1}{L^2}\left\langle\sum n_i\right\rangle, \tag{20}$$

its susceptibility $\chi_{\rho,L}$, the fourth-order cumulant $U_{\rho,L}$, as well as the energy (per lattice site), $\langle e\rangle$ and the heat capacity, C_V, obtained from the fluctuation theorem:

$$C_V = \frac{1}{kT^2}[\langle H^2\rangle - \langle H\rangle^2] \tag{21}$$

From the point of view of symmetry classification, there is no essential difference between the $c(2\times2)_F$ and AF phases, because both of them are described by the same type of order parameter component (Ψ_3), only in the perfectly ordered structures the magnitude of this order parameter component is different. Thus we expect that between these structures lines of first-order transitions ending at the critical point are possible in the phase diagram, similar to the liquid-gas transition of a (lattice) gas, where also both phases have the same symmetry properties, while a line of critical points of second-order transitions evidently is not possible. This consideration is born out by the phase diagrams found below (Fig. 26). In contrast, lines of critical points are possible for the transition from the $c(2\times2)_F$ phase to the disordered phase (Figs. 25 and 26), from the SAF to the disordered phase (Fig. 25) and from the $c(2\times2)_{AF}$ to the $c(2\times2)_F$ phase, since all these phases differ in their symmetry properties.

Since we have assumed that $|V_B|$ is the unit of energy, the reduced temperature is defined as $T^*=kT/|V_B|$, and the reduced chemical potential is given by $\mu^*=\mu/|V_B|$.

In order to study the nature of different phase transitions predicted to occur when the temperature and/or the chemical potential are varied, we have applied the histogram reweight-

ing method[53,54] as well as the hyper-parallel tempering technique,[55,56] supplemented by the finite size scaling analysis.[50] These methods are known to be very well suited to determine the properties close to the phase transition points. In particular, the hyper-parallel tempering allows us to investigate several thermodynamic states in a single run. Due to much faster convergence and lower fluctuations, this method is much less time demanding than independently performed simulations at each state point.[55] The length of the MC runs ranged between 10^6 and 10^7 Monte Carlo steps, where 1 Monte Carlo step corresponds to one sweep over the entire lattice.

From the finite size scaling theory it follows[50,57] that in a finite system of the size $L\times L$ any second-order phase transition is rounded and shifted, so that the heat capacity and the order parameter susceptibility peaks reach their maximum values [$C_{V,max}(L)$ and $\chi_{max}(L)$, respectively] at the temperatures $T_C^*(L)$ and $T_\chi^*(L)$ which scale with the system size as

$$T_j^*(L) - T_c^* \propto L^{-1/\nu}, \quad j = C, \chi, \tag{22}$$

where T_c^* is the transition temperature in a macroscopic system and ν is the critical exponent of the correlation length. Moreover, the maximum values of the heat capacity and of the susceptibility are expected to scale with L as

$$C_{max}(L) \propto L^{\alpha/\nu} \tag{23}$$

and

$$\chi_{max}(L) \propto L^{\gamma/\nu}, \tag{24}$$

where α and γ are the critical exponents of the heat capacity and susceptibility, respectively.

In order to use the relation (22) to estimate ν one needs very accurate estimations of $T_j^*(L)$, for a series of systems of different L, as well as an *a priori* knowledge of the true transition temperature T_c^*. Usually, the differences $T_j^*(L) - T_c^*$ are two or more orders of magnitude smaller than both $T_j^*(L)$ and T_c^*, so that even small errors in the estimations of $T_j^*(L)$ and T_c^* may produce large errors of ν.

However, the true transition temperature, T_c^*, can be determined independently from the plots of $U_{\Psi,L}(T)$ vs. T, obtained for various values of L, since all such curves have a common intersection point, the fixed point value of U^*, at T_c^*. Once the fourth-order cumulants for the systems of various L are known, one can also determine the critical exponent ν, using the relation at T_c^*,

$$\frac{\partial U(L)}{\partial(1/T)} \propto L^{1/\nu}, \tag{25}$$

if the corrections to scaling can be neglected.

IV. SYSTEMS WITH NONREPULSIVE FIRST-NEAREST NEIGHBOR INTERACTION

We begin the discussion with the presentation of results obtained for the systems in which Δu_2 is lower than, or equal to, zero. This assumption leads to a particularly simple situation. The only ordered states that can appear are the *F* and *AF* phases, which both should belong to the universality class of the two-dimensional Ising model.[58] At the ground state, the transition from the regime in which the *F* ordered structure is stable to the regime corresponding to the stable *AF* ordered structure is entirely determined by the values of ΔV and Δu_1 (cf. Fig. 2) and is located at the point $\Delta u_1/\Delta V = 0.25$. Thus, the formation of the *AF* structure requires the interaction between differently oriented molecules to be considerably stronger than the interaction between a pair of nearest neighbor molecules which have the same orientation.

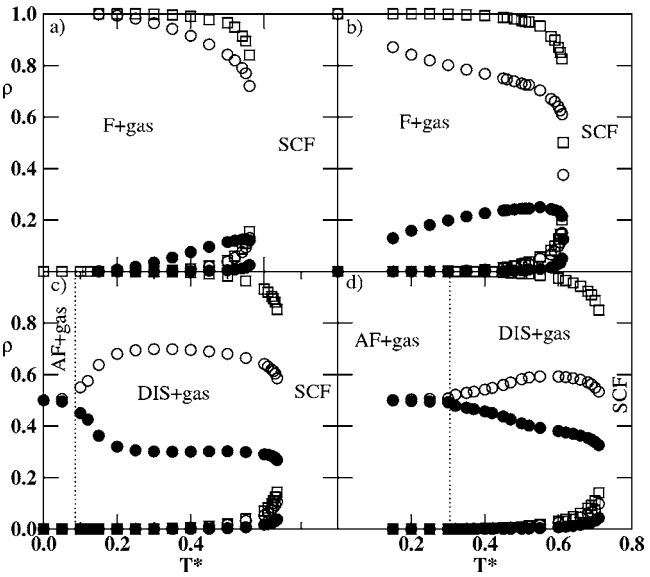

FIG. 3. Phase diagrams, in the density-temperature plane, obtained for the systems characterized by $u_{1,a}=-1.0$, $u_{2,a}=u_{2,b}=0.0$ and different values of $u_{1,b}=-1.0$ (a), -1.2 (b), -1.3 (c), and -1.5 (d). Open and filled circles mark the coexistence points for the molecules with $s_i=1$ and -1, respectively, while squares give total densities at the coexistence points. The phase diagrams have been evaluated using the simulation cell of the size 60×60. The verical dotted lines in (c) and (d) mark the temperatures of the transition between the AF and the disordered (DIS) phases. The region labelled by SCF corresponds to the supercritical fluid phase. Error bars have been omitted since the usual errors are not larger than the symbol size.

Figure 3 shows the examples of phase diagrams obtained for the systems in which only the interactions between the first-nearest neighbors are taken into account. Thus, we have assumed that $u_{2,a}=u_{2,b}=0$, $u_{1,a}=-1.0$ while $u_{1,b}$ assumed different values equal to $-1.0(\Delta u_1=0.0)$ [part (a)], $-1.2(\Delta u_1=0.2)$ [part (b)], $-1.3(\Delta u_1=0.3)$ [part (c)], and $-1.5(\Delta u_1=0.5)$ [part (d)]. For our choice of the parameters, the parts (a) and (b) of Fig. 3 present the phase diagrams for the systems which order into the phase *F*, while parts (c) and (d) correspond to the systems ordering into the phase *AF*. The depicted phase diagrams show that upon the increase of temperature, the ordered phases (*F* as well as *AF*) lose a perfect order at rather low temperatures, well below the respective critical points. Figure 4 presents the examples of the heat capacity curves for the systems which order into the structure *F* [Fig. 4(a)] and *AF* [Fig. 4(b)], obtained for a series of

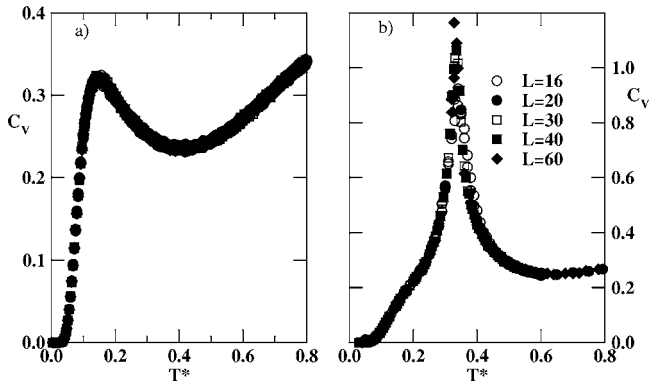

FIG. 4. The heat capacity versus temperature obtained for different sizes of the simulation cell [shown in (b) of the figure] and the systems characterized by $u_{1,a}=-1.0$, $u_{2,a}=u_{2,b}=0.0$ and the values of $u_{1,b}$ equal to -1.15 (a) and -1.4 (b). The results depicted here have been obtained at $\mu^*=-3.0$. In (a) errors are not larger than the symbol size. In (b) the error bars have been omitted for clarity. The largest error of C_V, close to the position of the peak maximum, does not exceed 0.08.

systems of different sizes of the simulation cell [see legend in Fig. 4(b)], and calculated at the fixed chemical potential value, well above the transition from the gas to the condensed phase transition. It should be noted that the calculations performed at other values of the chemical potential, but also above the gas-condensed phase transition point, lead to quite similar results, and, in particular, to almost the same locations and heights of the heat capacity maxima. When $\Delta u_1 < 0.25$ we observe rather broad heat capacity peaks without any finite size effects. Quite similar results have been obtained for the order parameter, Ψ_4, and the corresponding susceptibility, while the fourth-order cumulant of the order parameter exhibits gradually decreasing deviations from the trivial fixed point value of $\frac{2}{3}$ when the simulation cell size increases. Therefore, one concludes that the structure F disorders gradually. This gradual disordering in no surprise, since the system corresponds to a ferromagnet in an external field (due to the interaction with the substrate). For the antiferromagnetic structure, there is no linear coupling of the field to the order parameter, and hence a transition is still possible. Consistent with this argument, the results obtained for the system with $\Delta u_1 > 0.25$ [Fig. 4(b)] suggest that a continuous order-disorder phase transition occurs. Indeed, we have found that the heat capacity value at the maximum ($C_{V,max}$) diverges logarithmically with L [see Fig. 5(a)], and the scaling of susceptibility of the order parameter Ψ_3 [see Fig. 5(b)], according to the finite size scaling relation

$$\chi_{\Psi,L}(T) = L^{\gamma/\nu}\chi_o(|t|L^{1/\nu}), \tag{26}$$

where $t=|T-T_c|/T_c$ gives the values of the critical exponents $\nu=1.0$ and $\gamma=1.75$, as expected for the two-dimensional Ising model. Also, the behavior of the fourth-order cumulant of the order parameter (Ψ_3) confirms that the order-disorder transition belongs to the universality class of the two-dimensional Ising model. Namely, the cumulant fixed point at the transition temperature is known and equal to U^*

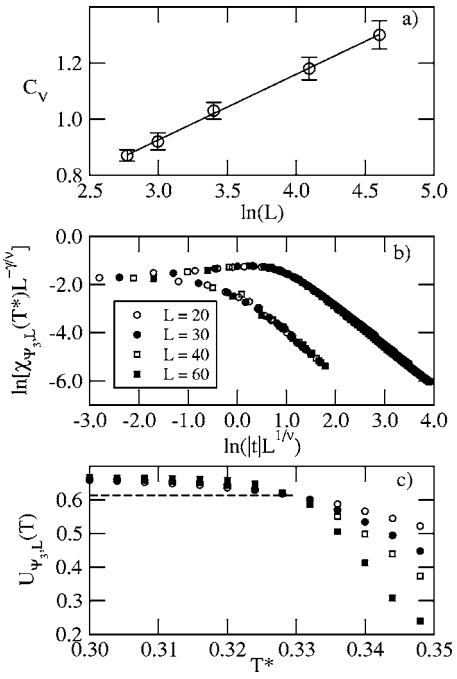

FIG. 5. The plot of $C_{V,max}$ vs. $\log L$ (a), the scaling plot of the order parameter susceptibility for the simulation cell sizes shown in the figure (b), and the temperature changes of the fourth-order cumulant for different sizes of the simulation cell [shown in (b)] (c) obtained for the system characterized by $u_{1,a}=-1.0$, $u_{2,a}=u_{2,b}=0$, and $u_{1,b}=-1.4$, obtained at $\mu^*=-3.0$.

≈ 0.610,[59] while our results [see Fig. 5(c)] give $U^*=0.613\pm0.004$. Of course, the temperature of the order-disorder transition as well as the location of the critical point of the gas-condensed phase transition (T_c^*) both depend on the magnitude of Δu_1. The lower panel of Fig. 6 shows the temperature, T_o^*, at which the heat capacity peaks of the ordered phase F reaches maximum (open circles) and the tem-

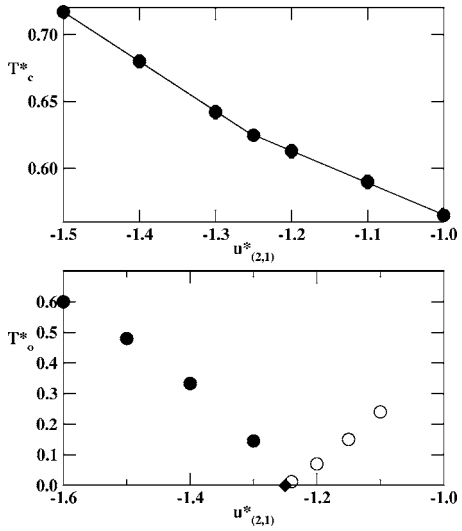

FIG. 6. The changes of the critical temperature, T_c^* (upper panel), and of the temperature at which the heat capacity reaches maximum, T_o^* (lower panel), vs. Δu_1 for the systems characterized by $u_{1,a}=-1.0$ and $u_{2,a}=u_{2,b}=0.0$.

TABLE III. The results of phenomenological renormalization for the system characterized by $u_{1,a}=-1.0$ and $u_{1,b}=-1.2$ ($\Delta u_1=0.2$) and $u_{2,a}=u_{2,b}=0.0$.

L_1	L_2	γ/ν
12.0	16.0	1.745
12.0	20.0	1.750
12.0	30.0	1.746
12.0	40.0	1.747
16.0	20.0	1.757
16.0	30.0	1.747
16.0	40.0	1.747
20.0	30.0	1.741
20.0	40.0	1.744
30.0	40.0	1.748

perature of the order-disorder transition of the condensed phase *AF* (filled circles) plotted against $u_{1,b}$, while the upper panel of Fig. 6 presents the changes of the critical temperature of the gas-condensed phase transition (T_c^*), also plotted as a function of $u_{1,b}$. One finds that T_o^* converges to zero when $u_{1,b}$ approaches $-1.25(\Delta u_1=0.25)$ from below. Also, the location of the heat capacity maximum, for the systems which order into the phase *F*, goes to zero when $u_{1,b}$ approaches -1.25 from above. Of course, only for $\Delta u_1>0.25$ we have a true order-disorder phase transition. On the other hand, the critical temperature of the gas to condensed phase transition linearly increases with $u_{1,b}$, since it is expected to be proportional to the total energy of the admolecule-admolecule interaction. The only effect of the crossover between the regimes in which the ordered phase has a different structure is a slight change of the slope of T_c^* versus $u_{1,b}$ line.

The critical behavior of the two-dimensional gas-condensed phase transition has been found to be also consistent with the predictions for the two-dimensional Ising model universality, when the condensed phase is either *F* or *AF* at the ground state. The cumulant fixed point has been found to be located at $U^*\approx 0.613$. The above conclusion has also been confirmed by the phenomenological renormalization, based on the following relation,[60]

$$\gamma/\nu=\frac{\ln[\chi_{\Psi_4,bL}(T_c)/\chi_{\Psi_4,L}(T_c)]}{\ln b}, \tag{27}$$

and the results obtained for the system characterized by $\Delta u_1=0.20$ are given in Table III. One readily notes that the ratio γ/ν takes on the values very close to the exact result for the two-dimensional Ising model, i.e., $\gamma/\nu=1.75$, with $\gamma=1.75$ and $\nu=1.0$. Quite similar results have been obtained for other systems characterized by different values of Δu_1, lower as well as higher than 0.25.

When the interactions between the second-nearest neighbors are added and assumed to be such that the system still orders into either *F* or *AF* phase, the qualitative picture does not change. Again, we find that the phase *F* gradually disorders at low temperatures and that the phase *AF* undergoes an Ising-like order-disorder transition. Also, the behavior in the vicinity of the critical point remains unchanged and the gas-condensed phase belongs to the universality class of the two-dimensional Ising model.

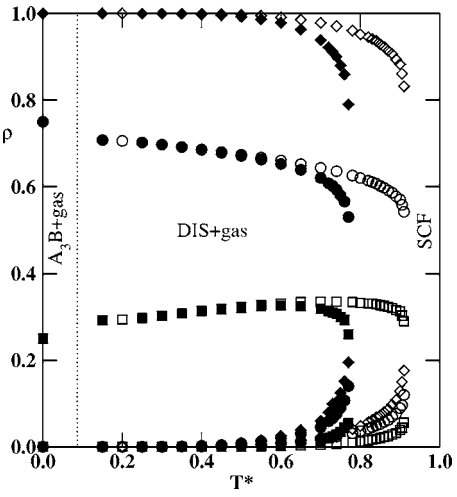

FIG. 7. The phase diagrams for the system characterized by $u_{1,a}=-1.0$, $u_{1,b}=-1.2$ ($\Delta u_1=0.2$) and the fixed value of $\Delta u_2=0.2$, but the different values of $u_{2,a}=-0.1$ and $u_{2,b}=-0.3$ (filled symbols) and $u_{2,a}=-0.3$ and $u_{2,b}=-0.5$ (open symbols). Circles and squares mark the coexistence points for the molecules with $s_i=1$ and -1, respectively, while diamonds give total densities at the coexistence points. The verical dotted line marks the temperature at which the A_3B phase undergoes a transition to the disordered phase (DIS). The region labelled by SCF corresponds to the supercritical fluid phase.

The situation changes when the values of Δu_1 and Δu_2 are chosen in such a way that the model predicts the formation of one of the ordered structures A_3B or *SAF* (cf. Fig. 2) at the ground state. Here, we consider a series of systems characterized by the values of Δu_1 and Δu_2, leading to the formation of the above-mentioned ordered phases A_3B or *SAF*, and assume that the interaction energies between the first-nearest neighbors ($u_{1,a}$ and $u_{1,b}$) are both nonrepulsive. At first, we consider the systems which order into the state A_3B. Figure 7 presents two examples of phase diagrams obtained for the systems characterized by the same values of $\Delta u_1=0.2$ and $\Delta u_2=0.2$, but with different values of the interaction energies $u_{2,a}$ and $u_{2,b}$. The first-nearest neighbor interaction energies have been equal to $u_{1,a}=-1.0$ and $u_{1,b}=-1.2$ in both cases, while the magnitudes of the second-neighbor interaction energies have been equal to $u_{2,a}=-0.1$ and $u_{2,b}=-0.3$ or $u_{2,a}=-0.3$ and $u_{2,b}=-0.5$. One readily notes that these two systems have different critical temperatures, while the low-temperature parts of the phase diagrams are quite the same in both cases. Qualitatively the same phase diagrams have been obtained for other systems, which order into the phase A_3B at low temperatures. In all such cases we have found that the ordered structure is stable only at very low temperatures and undergoes a disordering transition well below the critical point of the phase transition between the gas and the condensed phase. The nature of this order-disorder transition has been studied using a standard Monte Carlo simulation method in the grand canonical ensemble as well as with the help of the hyper-parallel tempering method in the grand canonical ensemble. It should be noted that independent ca-

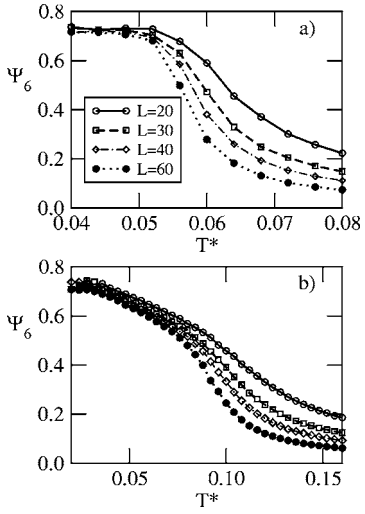

FIG. 8. Temperature changes of the order parameter Ψ_6 for different sizes of the simulation cell (shown in the figure) calculated for the systems characterized by $u_{1,a}=-1.0$, $u_{1,b}=-1.25$, $\Delta u_1=0.25$, $u_{2,a}=0.0$, and different values of $u_{2,b}$ equal to $-0.1(\Delta u_2=0.1)$ (a) and $-0.2(\Delta u_2=0.2)$ (b).

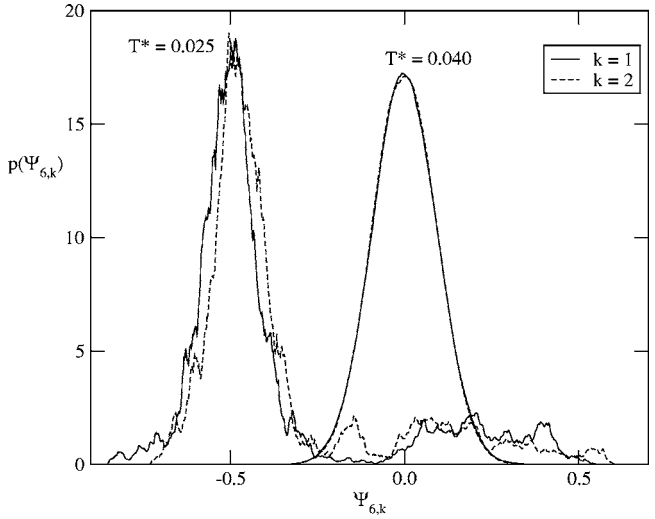

FIG. 9. Distributions of the order parameter components $\Psi_{6,1}$ and $\Psi_{6,2}$ for the system characterized by $u_{1,a}=-1.0$, $u_{1,b}=-1.25$, $u_{2,a}=0.0$, and $u_{2,b}=-0.05$ and $L=100$ at $\mu^*=-2.5$ and at two temperatures (shown in the figure).

nonical ensemble Monte Carlo simulations, performed under the condition of a completely filled lattice, give quite the same results. We have studied the behavior of the order parameter Ψ_6, the conjugated susceptibility, as well as the fourth-order cumulant for a series of systems, characterized by different values of Δu_2, while keeping Δu_1 fixed and equal to 0.25.

From the examples of the temperature changes of the order parameter Ψ_6, given in Fig. 8, one readily notes that Ψ_6 does not converge to unity when the temperature is decreased, but rather approaches the values close to $1/\sqrt{2}$ (in particular for large systems). This finding results from the fact that the structure A_3B is degenerate and each row containing up and down spins can be shifted by one lattice site without any energy penalty. Besides, the rows of up spins can be differently oriented, along x as well as y axis. Therefore, the simulations do not give a perfect A_3B structure, but rather a fluctuating domain structure, in which the $S_i=-1$ molecules occupy different sublattices. Since, the average contributions due to differently oriented domains are roughly the same, the components of the order parameter $\Psi_{6,1}$ and $\Psi_{6,2}$ both converge to about 0.5 (or -0.5), rather than to unity and hence Ψ_6 converges to $1/\sqrt{2}\approx 0.7071$ as is illustrated by the results presented in Fig. 8. Figure 9 shows two examples of the histograms of the order parameters $\Psi_{6,1}$ and $\Psi_{6,2}$ obtained at the temperatures below and above the order-disorder transition for the system ordering into the structure A_3B. One readily notes that below the transition temperature, the two components of the order parameter Ψ_6 exhibit sharp peaks around -0.5. It should be emphasized that the histogram of the order parameter, recorded at the temperature below the order-disorder transition (at $T^*=0.025$), is not smooth, despite that a very long run of 10^9 Monte Carlo steps has been performed. A particularly poor convergence of the order parameter has been observed for the systems with small values of Δu_2, lower than about 0.1, and small simulation cells of $L<60$. Therefore, we have not been able to obtain reliable estimations of the critical exponents for small values of Δu_2, despite very large computational efforts. Nevertheless, the results of the finite size scaling analysis provide a rather strong evidence that the order-disorder transition changes the universality class when Δu_2 increases. In the case of $\Delta u_2=0.1$ and 0.15 the cumulant fixed point and the critical exponents γ and ν assume the values consistent with the universality class of the Ising model. When, however, the parameter Δu_2 increases to 0.2 we find a quite different behavior. The fixed point of the order parameter cumulant assumes the value of 0.658 ± 0.001 (see Fig. 10) and the critical exponents γ and ν are equal to $\gamma=3.38\pm0.08$ and $\nu=1.87\pm0.04$, i.e., are considerably higher than in the case of the Ising universality class. When the value of Δu_2 increases further towards the threshold value of 0.25, which delimits the regions of stability of the ordered phases A_3B and *SAF*, the transition temperature gradually decreases. Thus, one can expect that it goes to zero when Δu_2 approaches 0.25.

As soon as the value of Δu_2 becomes higher than 0.25 the system orders into the structure *SAF* at the ground state. The symmetry of that ordered state is the same as the symmetry of the (2×1) phase, and it is known that the order-disorder transition of the (2×1) phase belongs to the universality class of the *XY* model with cubic anisotropy.[61] Therefore, one expects the critical exponents to be nonuniversal.[58] Below, we present the results which demonstrate that the critical exponents are in fact nonuniversal and depend on the magnitude of Δu_2.

The recorded temperature changes of the order parameter Ψ_{SAF} and of the corresponding fourth-order cumulant, obtained for different sizes of the simulation cell and the systems characterized by the fixed value of $\Delta u_1=0.2$ and different values of Δu_2, provide a strong evidence that all systems undergo a sharp order-disorder transition and that the fixed point values of cumulant U_L^* are considerably higher than

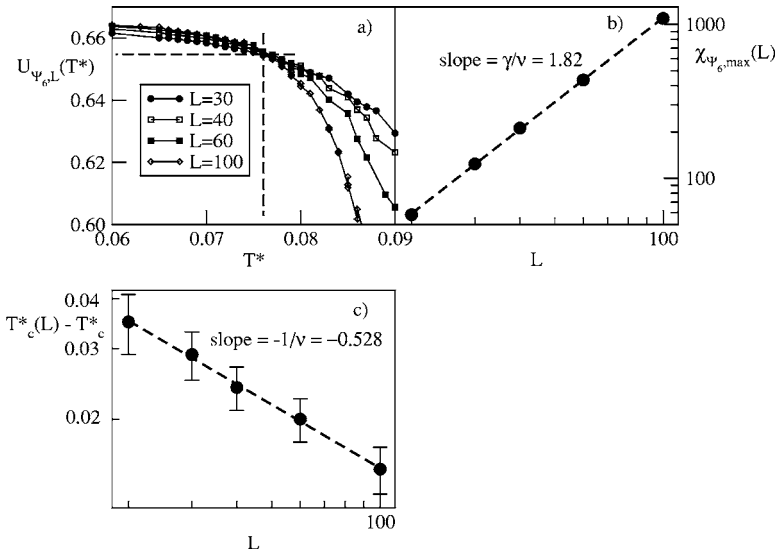

FIG. 10. Temperature changes of the fourth-order cumulant of the order parameter (a), log-log plot of the susceptibility maximum value $[\chi_{\Psi_6,max}(L)]$ versus L (b), and the log-log plot of $T_c^*(L)-T_c^*$ vs. L (c), for $\Delta u_2=0.20$, obtained from the hyper parallel tempering grand canonical Monte Carlo simulations, for $\Delta u_1=0.25$ at $\mu^*=-3.0$. Dashed lines in (a) mark the location of the transition point and the fixed point value of the cumulant.

predicted for the two-dimensional Ising model.

Figure 11 presents the results of the finite size scaling analysis, based on the relation (26), obtained for the system characterized by $\Delta u_1=0.2$ and $\Delta u_2=0.3$ ($u_{2,a}=0.0$, $u_{2,b}=-0.3$), which clearly demonstrate that the critical exponents $\nu=1.12\pm0.01$ and $\gamma=2.034\pm0.005$ are considerably higher than the values corresponding to the two-dimensional Ising model ($\nu=1$, $\gamma=1.75$). It is quite obvious that the scaling relation (26) is much better satisfied when nonuniversal values of the critical exponents are used.

Quite similar finite size scaling analysis has been performed for a number of systems characterized by different values of Δu_1 and Δu_2 and the results are summarized in Fig. 12, which shows the changes of the order-disorder transition temperature [part (a)], of the critical exponents γ [part (b)] and ν [part (c)], and of the cumulant fixed point value, U^* [part (d)], plotted versus Δu_2.

The above-presented results demonstrate that when the magnitude of Δu_2 exceeds about 0.4 the finite size scaling analysis leads to the critical exponents characteristic of the two-dimensional Ising model, though the fixed point value of the cumulant U^* does not converge to the value predicted for the two-dimensional Ising model, but to a considerably higher value of about 0.64. This may be related to particularly large corrections to scaling, so that still much larger simulation cells would be needed to reconcile the discrepancy. Such calculations would demand a prohibitively large amount of time. One should note, however, that the scaling analysis of the order parameter susceptibility, as well as of the heat capacity, confirm that for sufficiently large values of

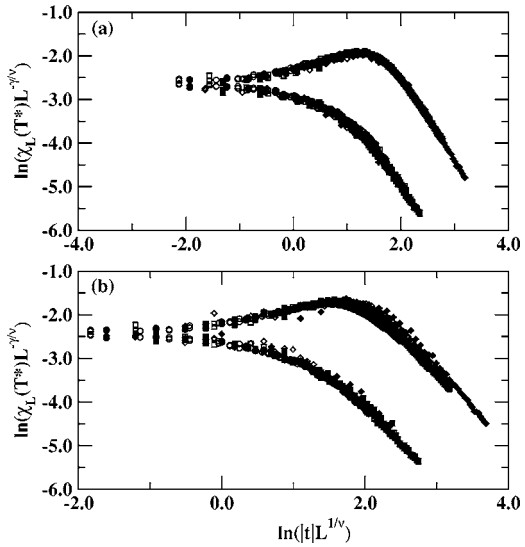

FIG. 11. The scaling plots of $\chi_L(T)L^{-\gamma/\nu}$ vs. $|t|L^{1/\nu}$ for the system characterized by $u_{1,a}=-1.0$, $u_{1,b}=-1.2$, $u_{2,a}=0.0$, and $u_{2,b}=-0.3$ for different values of the exponents $\nu=1.12$ and $\gamma=2.034$ (a) and $\nu=1.0$ and $\gamma=1.75$ (b). Different symbols denote the results obtained for different sizes of the simulation cell, $L=16$ (open circles), 20 (filled circles), 30 (open squares), 40 (filled squares), 60 (open diamonds), and 100 (filled diamonds).

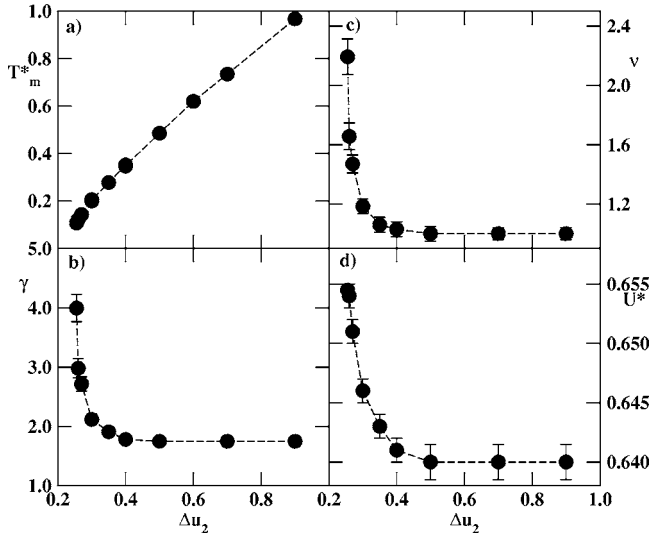

FIG. 12. The changes of the order-disorder transition temperature (a), of the critical exponents γ (b) and ν (c), and of the fixed point values of the fourth-order cumulant U^* against Δu_2, obtained for the systems characterized by $u_{1,a}=-1.0$, $u_{1,b}=-1.2$ ($\Delta u_1=0.2$), and $u_{2,a}=0.0$.

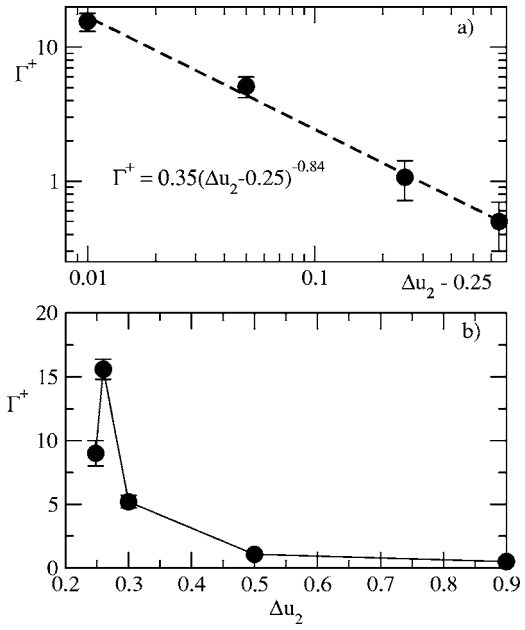

FIG. 13. (a) shows the log-log plot of the susceptibility amplitude Γ^+ vs. $\Delta u_2 - 0.25$, while (b) the plot of Γ^+ against Δu_2, for the systems with $\Delta u_1 = 0.25$.

Δu_2 the critical exponents correspond to the Ising universality class. Taking into account a rather limited accuracy of the critical exponents estimations and the fact that the cumulant fixed point at the transition temperature seems to be definitely larger than the value predicted for the Ising universality class, we can tentatively conclude that the critical exponents asymptotically approach Ising values when Δu_2 increases and the transition remains nonuniversal. This statement is supported by the results of the scaling analysis of the susceptibility. Namely, from the scaling relation (26) it follows that when $x = |t| L^{1/\nu} \to \infty$, the scaling function $\tilde{\chi}(x)$ can be written as

$$\tilde{\chi}(x) = \hat{\tilde{\chi}} x^{-\gamma} \tag{28}$$

so that we arrive at

TABLE IV. The locations of the order-disorder transition for the A_3B phase obtained for the systems characterized by the values of $\Delta u_1 = 0.25$ and different values of Δu_2.

Δu_2	T_o^*
0.05	0.0275±0.0005
0.10	0.0551±0.0005
0.15	0.0772±0.0006
0.20	0.075±0.003
0.22	0.067±0.004
0.24	0.04±0.004
0.245	0.01±0.003

$$\chi_{\Psi,L}(T) = \Gamma^{\pm} |t|^{-\gamma}, \tag{29}$$

where $\Gamma^{\pm}$ is the amplitude of χ at low, Γ^-, and high, Γ^+, temperatures, respectively. We have estimated the magnitudes of $\Gamma^{\pm}$ for several systems ordering into the phase *SAF* and found that Γ^+ is about an order of magnitude higher than Γ^- and both strongly depend on Δu_2. In particular, we have found that Γ^+ is likely to diverge when $\Delta u_2 - 0.25$ approaches zero [see Fig. 13(a)].

The results presented in of Fig. 12(a) and the data given in Table IV show that the order-disorder transition temperatures, of the phases *SAF* and A_3B, both decrease when Δu_2 approaches the threshold value of $0.25/\Delta V$, i.e., equal to 0.25 for our choice of $\Delta V = 1.0$.

A careful analysis of the region in which the values of Δu_2 are slightly lower than 0.25 indicates that the model predicts the presence of two order-disorder phase transitions. The first is due to the transition between the A_3B phase, stable at very low temperatures, and the (stable at higher temperatures) *SAF* phase, while the second is associated with the disordering of the *SAF* phase. It is demonstrated by the results presented in Fig. 14, which show the temperature changes of the susceptibilities of the order parameters Ψ_6 and Ψ_{SAF} obtained for the system with $\Delta u_2 = 0.24$ and $\Delta u_1 = 0.25$. One finds that there are two maxima present, which corespond to the above-mentioned two phase transitions.

The data presented in Fig. 15, obtained for the system with $\Delta u_2 = 0.24$ and $\Delta u_1 = 0.25$, show that in the case of the

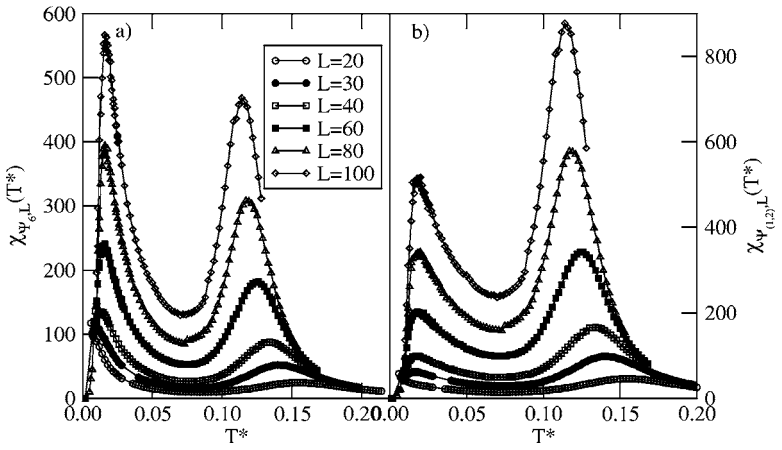

FIG. 14. Temperature dependences of the susceptibilities $\chi_{\Psi_6,L}$ (a) and $\chi_{\Psi_{SAF},L}$ (b) for the system with $\Delta u_2 = 0.24$ and $\Delta u_1 = 0.25$, obtained from the hyper-parallel tempering Monte Carlo simulation in the grand canonical ensemble at $\mu^* = -3.0$.

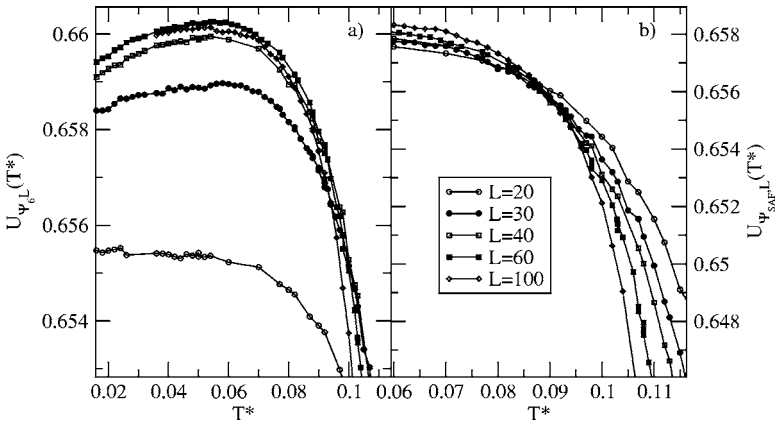

FIG. 15. Temperature dependences of the cumulants $U_{\Psi_6,L}$ (a) and $U_{\Psi_{SAF},L}$ (b) for the system with $\Delta u_2=0.248$ and $\Delta u_1=0.25$, obtained from the hyper-parallel tempering Monte Carlo simulation in the grand canonical ensemble at $\mu^*=-3.0$.

SAF order-disorder phase transition only the cumulants of the order parameter Ψ_{SAF} exhibit a nontrivial fixed point, $U^* \approx 0.655$ when $\Delta u_2=0.248$, while the cumulants of the order parameter Ψ_6 cross only for small systems, and do not when the size of the simulation cell becomes sufficiently large.

It should be also noted that the amplitude, Γ^+, of the susceptibility $\chi_{\Psi_{SAF}}(T)$, obtained for the system with $\Delta u_2=0.248$ is lower than in the case of Δu_2 slightly exceeding 0.25 [see Fig. 13(b)]. Also, the scaling analysis of the susceptibility, using the relation (26), and of the cumulants, according to the equation

$$U(L,T) \propto |t|L^{1/\nu}, \tag{30}$$

performed for the system with $\Delta u_2=0.248$ (see Fig. 16), show that the critical exponents $\gamma=3.8\pm0.2$ and $\nu=2.1\pm0.1$ are smaller than in the case of $\Delta u_2=0.255$, for which we have obtained $\gamma=3.94\pm0.15$ and $\nu=2.15\pm0.1$. These data suggest that the amplitude Γ^+ does not diverge, as suggested by the results given in of Fig. 13(a), but rather exhibit maximum value at Δu_2 close to 0.25.

From the above-presented results we have constructed the phase diagram, given in Fig. 17. This phase diagram has been calculated for a particular choice of $\Delta u_1=0.25$ and includes only the data obtained for positive values of Δu_2. Note that with the computer resources available to us it still was not possible to make a reliable statement where the line of the transition from the disordered phase to the SAF phase ends when one approaches the A_3B phase! When Δu_2 is negative the phase diagram should also involve the line of the order-disorder transition of the phase AF (when $\Delta u_1 > 0.25$), which begins at the value of Δu_2 depending on Δu_1 and equal to $\Delta\tilde{u}_2=\Delta u_1-0.25/\Delta V$, where $\Delta u_1 \in [0.25, 0.50]$. In such cases, the stability region of the phase A_3B also terminates at $\Delta\tilde{u}_2$ and the temperature of the order-disorder transition of the phase A_3B converges to zero at $\Delta\tilde{u}_2$. When Δu_1 is smaller than 0.25 the phase F sets in. This phase does not undergo any order-disorder transition and hence the phase diagram, shown in Fig. 17, terminates at the point $\Delta\tilde{u}_2=-\Delta u_1-0.25/\Delta V$, where $\Delta u_1 \in [0.0, 0.25]$.

Although we have not performed any systematic studies, the behavior of the model appears to be also dependent on the magnitude of Δu_1. For example, when $u_{1,a}=-1.0$, $u_{1,b}=-1.6$ ($\Delta u_1=0.6$) and $u_{2,a}=0.0$, $u_{2,b}=-0.4$ ($\Delta u_2=0.4$), the system orders into the SAF phase, but the nature of the order-transition changes, with respect to that corresponding to $\Delta u_1=0.25$ and $\Delta u_2=0.4$. In particular, the system with $\Delta u_1=0.6$ gives the order parameter cumulant fixed point equal to about $U^*=0.612\pm0.03$ (cf. Fig. 18), i.e., corresponding to the Ising universality class, while the system earlier discussed, with $\Delta u_2=0.25$, gives $U^* \approx 0.64$. Preliminary results obtained for larger and smaller values of Δu_2 equal to 0.45 and 0.37 suggest, however, that the transition is nonuniversal. In

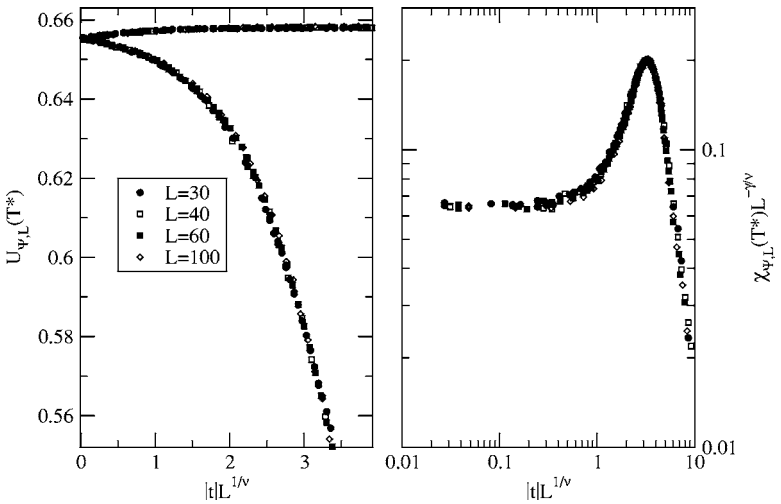

FIG. 16. Scaling plots of the fourth-order cumulant ($U_{\Psi_{SAF},L}$) and of the susceptibility ($\chi_{\Psi_{SAF},L}$) for the system with $\Delta u_1=0.25$ and $\Delta u_2=0.248$.

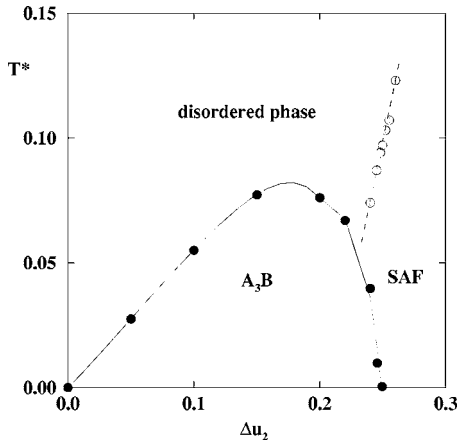

FIG. 17. The phase diagram obtained for the systems with $\Delta u_1=0.25$.

particular, the fixed point of the order parameter cumulant changes with both Δu_1 and Δu_2. The problem of the crossover between these different regimes is left for future study.

V. SYSTEMS WITH NONATTRACTIVE FIRST-NEAREST NEIGHBOR INTERACTION

In this section we assume again that $V_A=-2.0$ and $V_B=-1.0$, so that $\Delta V=1.0$, and consider two series of systems with $u_{1,a}=u_{1,b}=0.25$ ($\Delta u_1=0.0$) and with $u_{1,a}=0.5$, $u_{1,b}=0.0$ ($\Delta u_1=0.5$), i.e., the first-nearest neighbor interactions are assumed to be nonattractive. Moreover, we fix the parameter $u_{2,a}$ as equal to -1.0, assuming that the interaction energy between a pair of the next-nearest neighbors having the same orientation is attractive. Allowing the parameter $u_{2,b}$, and hence Δu_2, to vary, we consider two paths, marked by dots in Fig. 2. Thus, we exclude from the discussion the systems which can order into the A_3B structure in the ground state.

With our choice of the parameters $u_{k,l}$ ($k=1,2$ and $l=a,b$) the model predicts that at sufficiently low temperatures, the formation of a fully occupied monolayer should occur via a sequence of two first-order phase transitions. The first transition leads to the condensation of a dilute (gas-like) phase into one of the ordered states of the density $\rho=0.5$, $c(2\times2)_F$ or $c(2\times2)_{AF}$, depending on the magnitude of Δu_2. Then, upon a further increase of the chemical potential, the second transition to one of the ordered states (F, AF, or SAF) of the density $\rho=1.0$ takes place. Our first aim has been to locate the critical points of the above-mentioned transitions and to determine their universality classes. For this purpose we have applied the histogram reweighting method[53,54] together with a finite size scaling analysis.[15] The results are summarized in Figs. 19 and 20, which show how the critical parameters (T_c, ρ_c, μ_c, and U_ρ^*) change with Δu_2, when Δu_1 is equal 0.0 as well as 0.5. Figure 19 shows the critical parameters for the transition leading to the formation of the low density ($\rho=0.5$) phases, while Fig. 20 corresponds to the transitions between the low and high density phases. Parts (d) of both figures present the corresponding plots of the fixed point values of the fourth-order cumulant of the density, U_ρ^*, at the critical temperature.

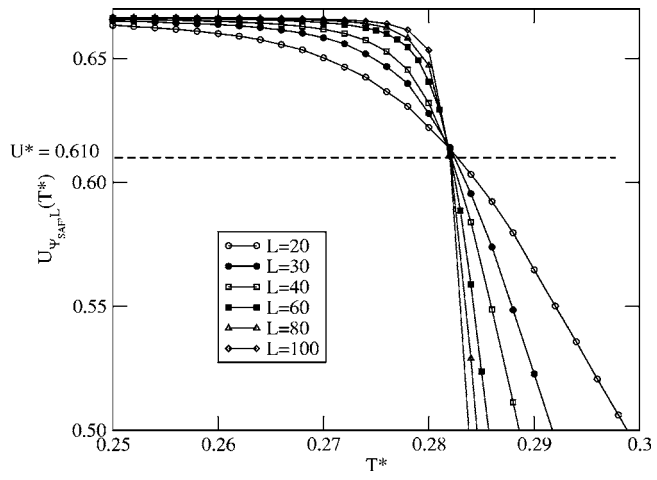

FIG. 18. Temperature dependences of $U_{\Psi_{SAF},L}$ for the system with $\Delta u_2=0.4$ and $\Delta u_1=0.6$, obtained from the hyper-parallel tempering Monte Carlo simulation in the grand canonical ensemble at $\mu^*=-3.0$.

The results given in Figs. 19 and 20 demonstrate that there are two regimes of Δu_2 in which both transitions exhibit a different behavior. For negative values of Δu_2 the critical temperature remains nearly constant, while for higher values of Δu_2 it increases. The fixed point value of the fourth-order cumulants U_ρ^*, at the critical points of the gas-$c(2\times2)_F$ as well as of the gas-$c(2\times2)_{AF}$ transitions [given in Fig. 19(d)], is independent of both Δu_1 and Δu_2 and takes on the values very close to about 0.57, suggesting that the transition belongs to the universality class of the tricritical point of the Blume-Capel (BC) model, for which the cumulant fixed point is equal to 0.574.[54] The fact that we have obtained slightly lower values of U_ρ^* can be attributed to finite size effects and neglected corrections to scaling. In order to confirm the prediction that the transition belongs to the tricritical universality class of the BC model, we have estimated the critical exponents β, γ, and ν using the finite size scaling analysis. The results obtained agree quite well with the exponents found in the study[54,62,63] of the BC model. Thus this finding implies that the phase coexistence ends at the tricritical point rather than at a critical point.

In the case of the second transition, between one of the low density ordered state [$c(2\times2)_F$ or $c(2\times2)_{AF}$] and the high density phase (F, AF, or SAF) we have also found two different regimes with respect to the variation of Δu_2 (cf. Fig. 20). In this case, however, we also find that for Δu_2 lower than zero the nature of the transition changes and depends not only on the magnitude of Δu_2, but also on Δu_1. When $\Delta u_1=0$ the ground state calculations predict that whenever $\Delta u_2/\Delta V$ is lower than 0.25 the transition occurs between the $c(2\times2)_F$ and F phase, while for higher values of the ratio $\Delta u_2/\Delta V$, the transition takes place between the phases $c(2\times2)_{AF}$ and SAF. The results given in Fig. 20, and in particular those presented in part (d), clearly demonstrate that there is a crossover between different regimes when Δu_2 is close to

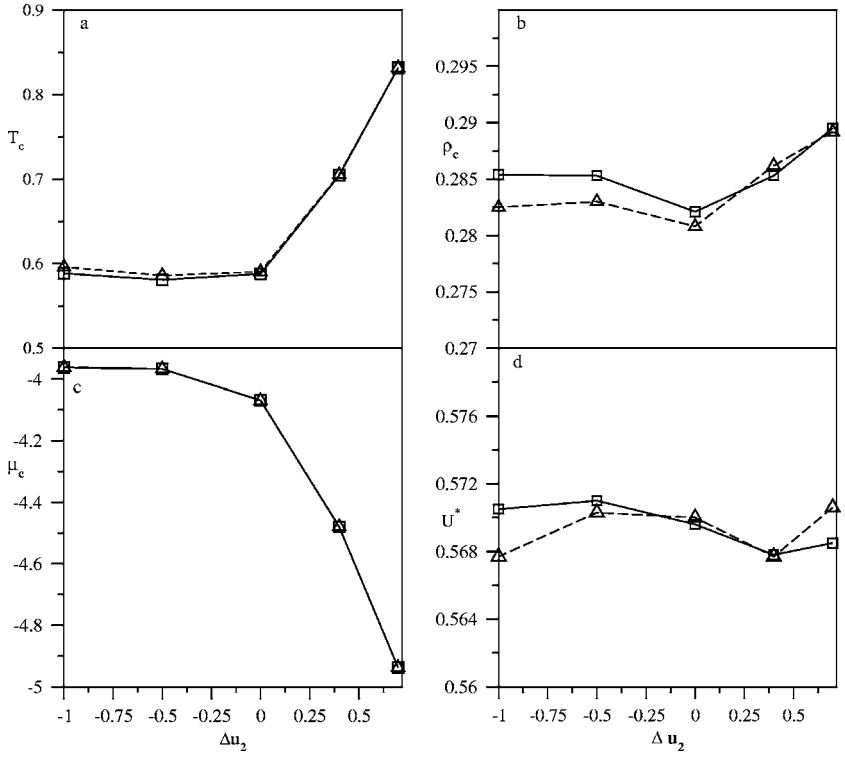

FIG. 19. The changes of the critical paremeters T_c (a), ρ_c (b), μ_c (c), and the fixed point of fourth-order density cumulant, U_ρ^* (d) vs. Δu_2, corresponding to the transition between the gas-like and the low density ordered structure $[c(2\times2)_F$ or $c(2\times2)_{AF}]$. Squares (triangles) correspond to the path with $\Delta u_1=0.0(0.5)$. Full and broken lines are guides to the eye only. In (a)–(c) the errors are not larger than the symbols size, while in (d) the largest error is equal to ±0.002, i.e., it is only slightly larger than the symbols size.

zero rather than about 0.25. In particular, the cumulant fixed point exhibits a jump from the BC tricritical universality class to the universality class of the two-dimensional Ising model,[64] when Δu_2 decreases from positive to negative values. On the other hand, no such crossover is observed when $\Delta u_1=0.5$, i.e., when the low-density ordered phase [either $c(2\times2)_F$ or $c(2\times2)_{AF}$] undergoes a transition to the high-density phase (either *AF* or *SAF*). In these two cases we again find that the transition belongs to the tricritical universality class of the BC model.

The results reported above have been based on the calculations of the fourth-order cumulant of the density rather than the order parameters, defined in Sec. III, suitable to detect different ordered structures.

In order to clarify the observed behavior we have performed the grand canonical Monte Carlo simulations and

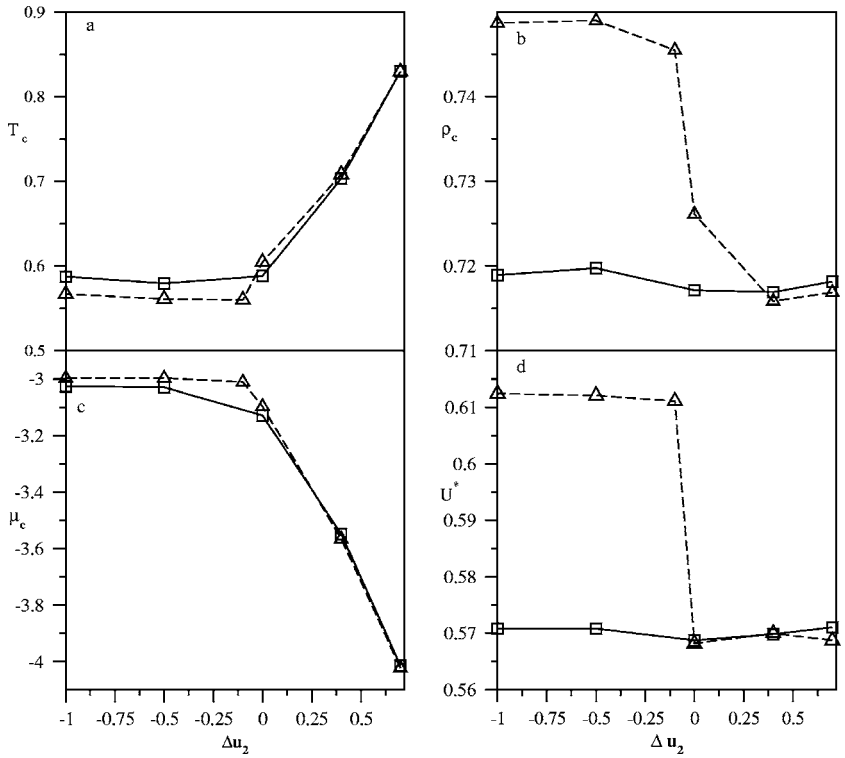

FIG. 20. The changes of the critical parameters T_c (a), ρ_c (b), μ_c (c), and the fixed point of fourth-order density cumulant, U_ρ^* (d) vs. Δu_2, corresponding to the transition between the low density $[c(2\times2)_F$ or $c(2\times2)_{AF}]$ and high density (*F*, *AF* or *SAF*) ordered structure. Squares (triangles) correspond to the path with $\Delta u_1=0.0(0.5)$. In (a)–(c) the errors are not larger than the symbols size, while in (d) the largest error is equal to ±0.002, i.e., it is only slightly larger than the symbols size.

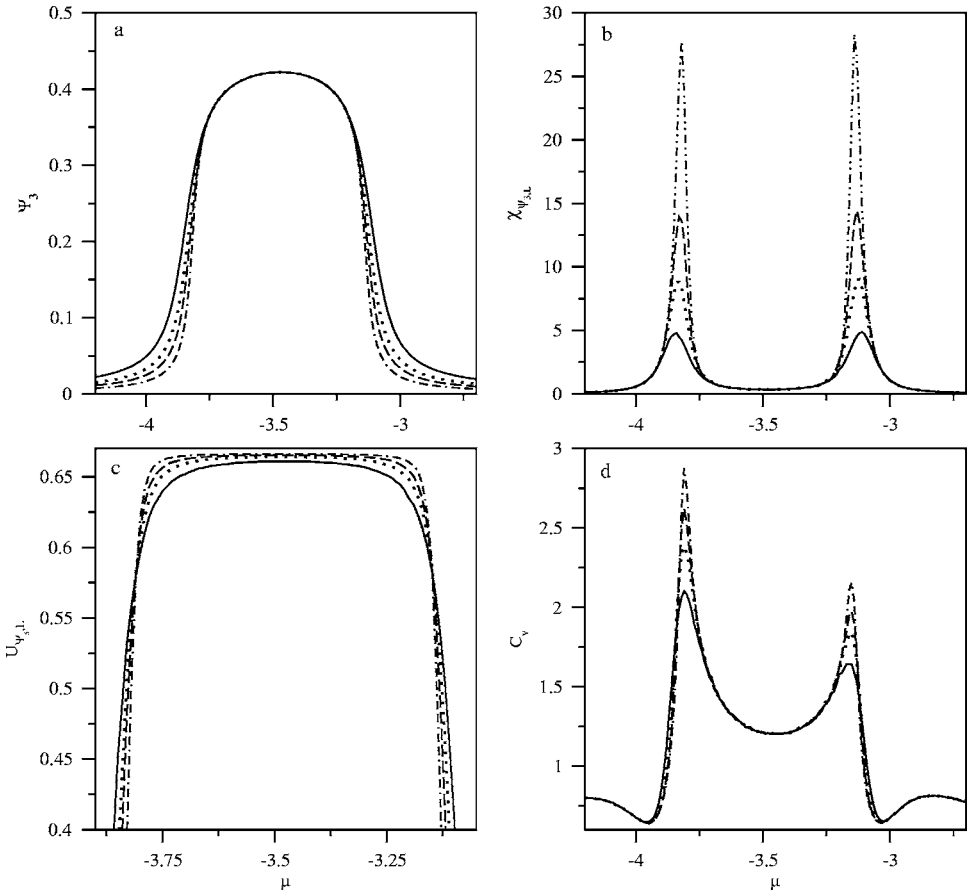

FIG. 21. The changes of the order parameter $\Psi_{3,L}$ (a), its susceptibility (b), and the fourth-order cumulant (c) as well as of the heat capacity (d) with the chemical potential at $T=0.75$ for different sizes of the simulation cell ($L=30$—solid lines, 40—dotted lines, 60—dashed lines, and 100—dashed-dotted lines) for the system with $\Delta u_1=0.0$ and $\Delta u_2=-1.0$.

recorded the order parameters Ψ_3 and Ψ_{SAF} as well as their distributions under different conditions.

Figure 21 presents the variation of several quantities with chemical potential, μ: the order parameter Ψ_3, the corresponding susceptibility, the fourth-order cumulant, and the heat capacity, using cells of different size and the system characterized by $\Delta u_1=0$ and $\Delta u_2=-1$. The results presented have been obtained from simulations performed at the temperature $T=0.75$, being considerably higher than the critical temperatures of both the dilute gas-like to $c(2\times2)_F$ and the $c(2\times2)_F$ to F transitions, which is equal to about 0.59 for the first transition and to about 0.57 for the second transition, respectively. It is quite transparent that there are two continuous phase transitions present. The first transition occurs between a dilute disordered (DIS) phase and the ordered $c(2\times2)_F$ phase, while the second occurs between the ordered $c(2\times2)_F$ phase and the high-density DIS phase, in which Ψ_3 vanishes again. The fixed point values of the order parameter cumulant, $U^*_{\Psi_3}$, are again equal to about 0.57 for both transitions. The appearance of the two continuous transitions at such high temperatures confirms that for the assumed values of the parameters we observe tricritical rather than critical points.

The situation is expected to be quite different when Δu_2 becomes larger than 0.25. The ground state considerations predict that in such cases the following transitions take place: the first transition is due to the condensation of a dilute gas-like phase into the ordered $c(2\times2)_{AF}$ phase, while the second transition occurs between the ordered structure $c(2\times2)_{AF}$ and the high-density *SAF* phase. The results given in Fig. 22(a) demonstrate, however, that at the temperature used ($T=0.95$) the order parameter Ψ_{SAF} goes to zero over the entire range of μ when the system size increases. Also the corresponding susceptibility [see Fig. 22(b)] does not exhibit finite size effects expected for a continuous phase transition. On the other hand, the order parameter Ψ_3 as well as the corresponding susceptibility, given in parts (c) and (d) of Fig. 22, both exhibit the behavior indicating the presence of two continuous transitions, and the fixed point value of the order parameter cumulant is again located at about 0.57. One should note, however, that the order parameter Ψ_3 is quite low in the ordered phase and reaches the maximum value of only about 0.065! The results are still more surprising since the value of Δu_2 (equal to 0.7) is considerably higher than the value predicted by the ground state calculations (equal to 0.25) above which the low density ordered structure should be $c(2\times2)_{AF}$ rather than $c(2\times2)_F$. Therefore, it seems that the boundary between the above two low-density ordered states drifts toward higher values of Δu_2 as the temperature increases. Note that the results given in Fig. 22 have been obtained at $T^*=0.95$, i.e., above the tricritical point, which is located at the temperature of about 0.84 (cf. Fig. 20). The results presented in Fig. 22 are also supported by the calculations of the order parameter distributions (shown in Fig. 23), obtained for three different values of $u_{2,b}$ equal to -1.0, -1.4, and -1.7, at the temperatures close to the tricritical points of these systems. Part (a) of Fig. 23 shows the distributions of Ψ_3, part (b) shows the distributions of the component Ψ_2 and of the order parameter Ψ_{SAF} (the distribution

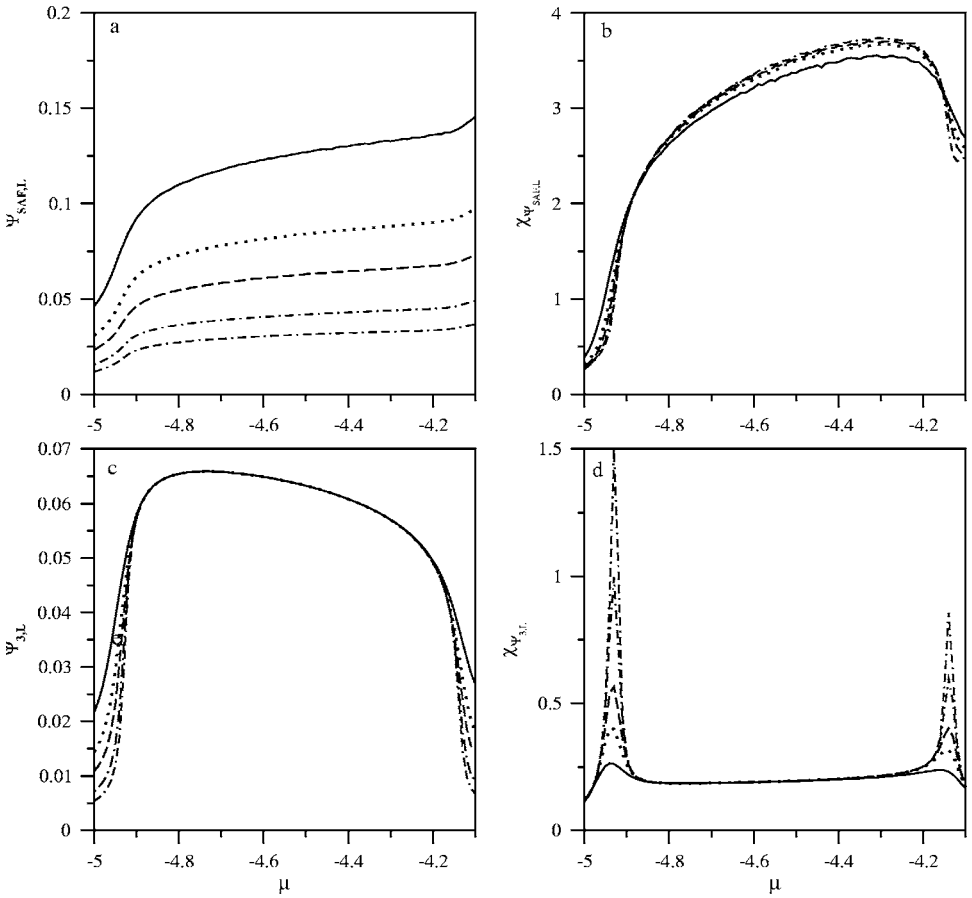

FIG. 22. The changes of the order parameter $\Psi_{SAF,L}$ (a) and $\Psi_{3,L}$ (c), and the corresponding susceptibilities [(b) and (d)] against the chemical potential at $T=0.95$ for the system with $\Delta u_1=0.0$ and $\Delta u_2=0.7$, obtained for different sizes of the simulation box ($L=30$—solid lines, 40—dotted lines, 60—dashed lines, and 100—dashed-dotted lines).

of the second component is the same) in the region of the transition between the low- and high-density ordered phases, at the average density close to about 0.75, while the lower panels [parts (c) and (d)] present the distributions of Ψ_3 and Ψ_2 in the region of the transition between a dilute (gas-like) and the low-density ordered phase, at the average density equal to about 0.25. In both cases, the distributions of Ψ_3 possess three maxima, one at $\Psi_3=0$ that comes from the disordered phases, and two maxima at $\pm\Psi_{3,o}(T)$ associated with the phase $c(2\times2)_F$. Of course, at the temperatures above the tricritical points, the distributions of the order parameter Ψ_3 exhibit two maxima, due to the presence of $c(2\times2)_F$ ordered structure. On the other hand, the distributions of Ψ_2 are, in all cases, simple Gaussians centered at $\Psi_2=0$, indicating a lack of the orderings characteristic to the phases $c(2\times2)_{AF}$ as well as *SAF*. One should note that at the ground state the systems with $u_{2,b}$ lower than -1.25 are expected to order into the above-mentioned ordered states $c(2\times2)_{AF}$ and *SAF*. This again suggests that the increase of temperature may cause a large shift of the threshold value of $u_{2,b}$, which delimits the regimes of different orderings. The canonical ensemble Monte Carlo calculations, performed at the density $\rho=0.5$ for a series of systems with $\Delta u_1=0.0$, and characterized by different values of Δu_2, equal to 0.3, 0.4 and 0.7, have shown, however, that there is a continuous phase transition between the $c(2\times2)_{AF}$ structure, which is stable at low temperatures, and the structure $c(2\times2)_F$, which is stable at higher temperatures. When the temperature increases further, the phase $c(2\times2)_F$ undergoes a transition to a disordered phase. The temperature of the transition between the $c(2\times2)_{AF}$ and $c(2\times2)_F$ phases gradually approaches zero when $\Delta u_2/\Delta V$ decreases toward 0.25 (see Fig. 24) and the transition belongs to the universality class of the two-dimensional Ising model. On the other hand, the temperature of the order-disorder transition of the $c(2\times2)_F$ phase depends on the density and reaches its maximum value at $\rho=0.5$. Quite similar canonical ensemble simulations have been performed at the density $\rho=1.0$ and demonstrated that the phase *SAF* is stable only at low temperatures and undergoes an order-disorder transition at the temperature well below the tricritical point. This transition is nonuniversal, as it was demonstrated in Sec. IV. In particular, the critical exponents ν and γ depend on the magnitude of Δu_2 and seem to asymptotically approach Ising values upon the increase of Δu_2. It should be noted that the transition temperature, equal to about 0.73 when $\Delta u_2=0.7$, agrees very well with the value obtained for the system with $\Delta u_1=1.2$ and $\Delta u_2=0.7$, but with completely different magnitudes of the interaction energies $u_{k,l}$, $(k=1,2)$ and $l=a,b$, equal to $u_{1,a}=-1.0$, $u_{1,b}=-1.2$, $u_{2,a}=0.0$, and $u_{2,b}=-0.7$ (see Sec. IV).

Using the results of the canonical ensemble simulations, as well as the results obtained from hyper-parallel tempering Monte Carlo simulations in the grand canonical ensemble, we have determined the phase diagram for the system characterized by $\Delta u_1=0.0$ and $\Delta u_2=0.7$, which is shown in Fig. 25. Parts (a) and (b) show the density-temperature and the temperature-chemical potential projections of the phase diagram, respectively. Solid lines mark the first-order transitions, while dotted and dashed lines mark the continuous

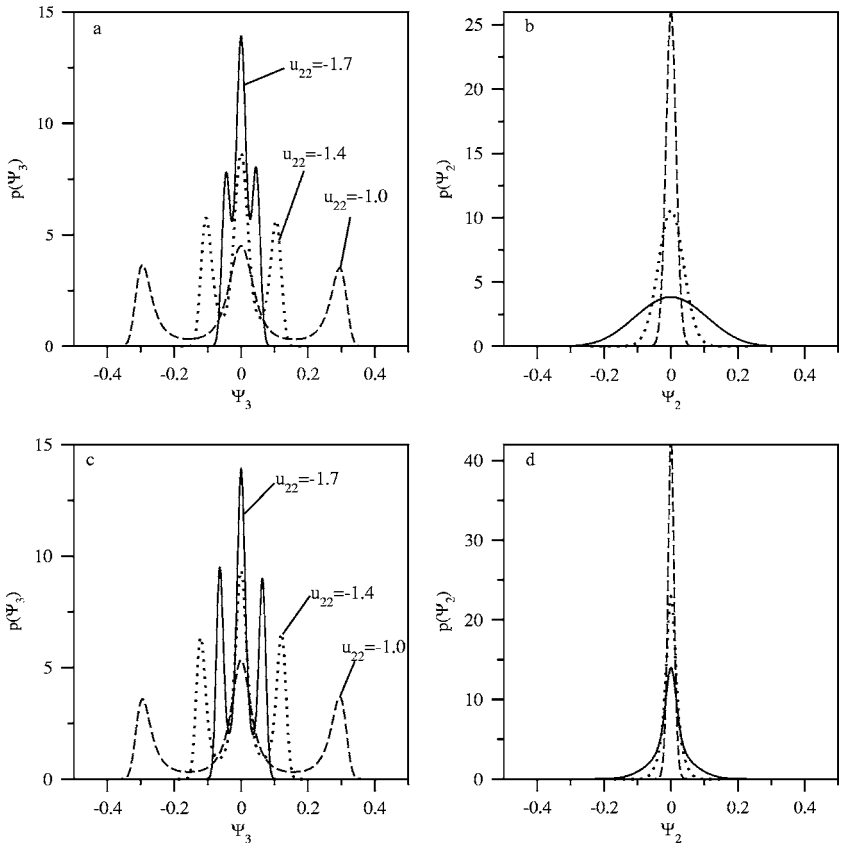

FIG. 23. Distributions of the order parameter Ψ_3 [(a) and (c)] and one of the components, Ψ_2, of Ψ_{SAF} [(b) and (d)], at the temperatures slightly lower that the tricritical point temperature and the chemical potential at the coexistence line for the systems with $\Delta u_1 = 0.0$ and different Δu_2 equal to 0.0 (dashed lines), 0.4 (dotted lines), and 0.7 (solid lines). Parts (a) and (b) refer to the transition from the $c(2\times2)_{AF}$ phase to the high density *SAF* phase, while (c) and (d) refer to the transition from the gas-like phase to the ordered $c(2\times2)$ structure.

transitions. The dotted lines correspond to the transitions between the $c(2\times2)_{AF}$ and $c(2\times2)_F$ as well as between the SAF and disordered high density phases. These two lines join the first-order transition boundaries at the respective critical end points (CEP's), $T_{e,1}$, $T_{e,2}$, and $T_{e,3}$.

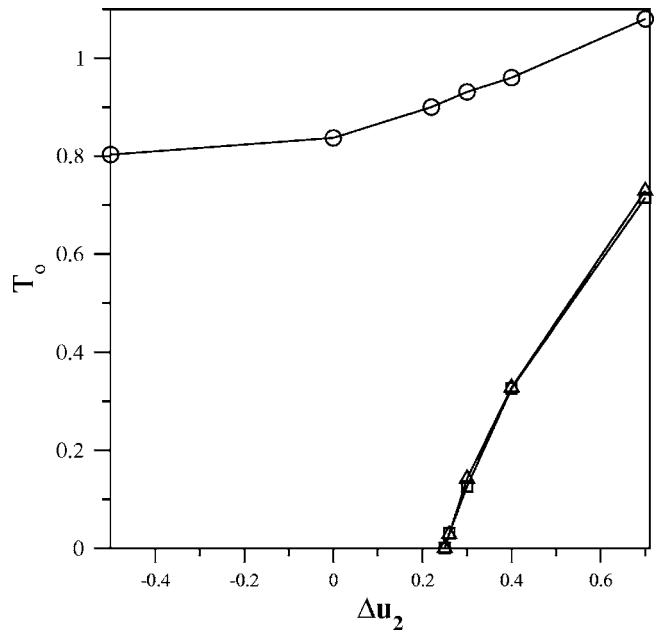

FIG. 24. The changes of the order-disorder transition temperatures for the phases $c(2\times2)_F$ (circles) and $c(2\times2)_{AF}$ (squares), and *SAF* (triangles) plotted against Δu_2, for the systems with $\Delta u_1 = 0.0$. Error bars have been omitted since the errors do no exceed the size of the symbols.

Qualitatively the same phase diagrams occur when the parameter Δu_2 is varied, but stays above 0.25. The only effects of the variation of Δu_2 are the shifts of the phase boundaries. Thus, the critical end points, $T_{e,1}$, $T_{e,2}$, and $T_{e,3}$, both the tricritical points, $T_{trc,1}$ and $T_{trc,2}$, as well as the maximal critical point, $T_{c,max}$, all are shifted to lower values when Δu_2 decreases towards 0.25. One should note that the lines of the critical points, presented in Fig. 25, associated with the transitions $c(2\times2)_{AF}$-$c(2\times2)_F$ and *SAF*-disordered phase (dotted lines), both exhibit a very strong temperature dependence. The line of the transition $c(2\times2)_{AF}$-$c(2\times2)_F$ terminates at the coexistence curve of the first-order transition leading to the high-density disordered phase, at $T_{e,3}$. Also the line of the phase transition from the *SAF* to the disordered phase terminates at a finite temperature, at which the density reaches unity.

As soon as Δu_2 becomes lower than 0.25 the topology of the phase diagram changes, since the ordered structures $c(2\times2)_{AF}$ and *SAF* are not present, as it also follows from the ground state considerations. Thus, the phase diagram exhibits only the first-order transitions; the first between a gas and $c(2\times2)_F$ phases, and the second between the $c(2\times2)_F$ and the ferromagnetic-like phases. We do not call it the *F* ordered structure, since it has rather special properties. Namely, the magnetization (Ψ_4) approaches the same value as the density and it does not exhibit an order-disorder phase transition, as it was demonstrated in Sec. IV. This special behavior results from the assumed external (surface) field which causes a

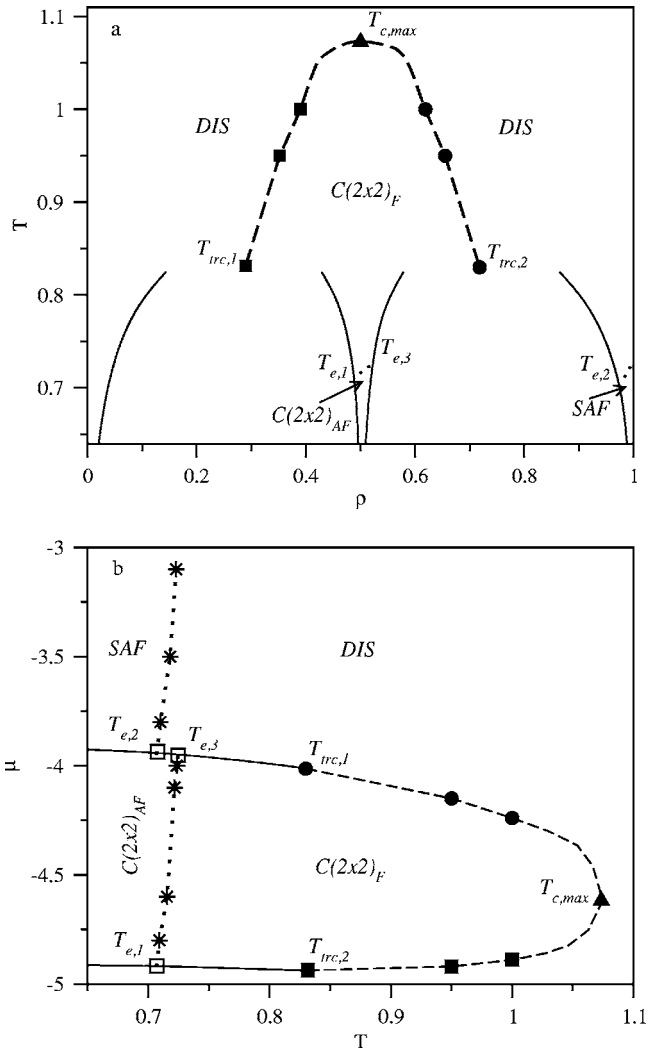

FIG. 25. The density-temperature (a) and the temperature-chemical potential (b) projections of the phase diagram for the system with $\Delta u_1=0.0$ and $\Delta u_2=0.7$. The critical endpoints are highlighted as open squares in (b).

preferential orientation of the molecules with the spins $S_i=+1$, even at elevated temperatures.

The next series of calculations have been performed for the systems with $\Delta u_1=0.5$ and different values of Δu_2 ranging from -1.0 to 0.7. As long as Δu_2 stays below zero the only possible ordered phases are the $c(2\times2)_F$ and *AF*. The first-order transition between a dilute gas-like phase and the ordered $c(2\times2)_F$ phase terminates at the tricritical point, so that at higher temperatures there exists a line of a continuous transition between the disordered and the ordered $[c(2\times2)_F]$ phases. On the other hand, the subsequent transition between the $c(2\times2)_F$ and the *AF* ordered structures is of first order and terminates at the critical point, which belongs to the universality class of the two-dimensional Ising model. In parts (a) and (b) of Fig. 26 we present two phase diagrams, obtained for different values of $\Delta u_2=-0.5$ and -0.1, respectively. The topology of these two phase diagrams is the same. The only effects of the increase of Δu_2 is a gradual lowering of the temperature at which the ordered *AF* structure of density close to, and equal to, unity undergoes an order-disorder phase transition. The temperature at which this transition takes place decreases when Δu_2 approaches the value which delimits the regions of stability of different ordered phases at $T=0$. In the present case, with $\Delta u_1=0.5$, the stability of the phase *AF* terminates at $\Delta u_2=0.25$. The order-disorder transition of the phase *AF* is known to belong to the universality class of the 2D Ising model.[64] Also the order-disorder transition of the low density $c(2\times2)_F$ phase belongs to the same universality class. On the other hand, the tricritical point, at which the line of the order-disorder phase transition begins, belongs to the tricritical universality class, of course. Therefore, there is a sudden change of the critical exponents and other universal properties at the tricritical point. This is demonstrated in Fig. 27, which shows the magnitudes of the order parameter cumulant intersection point at the order-disorder phase transition as a function of temperature for the system with $\Delta u_2=-0.5$. One readily notes that the cumulant intersection point at the tricritical point has the value very close to 0.574, while at the temperatures well above this point it assumes the values corresponding to the 2D Ising universality. We must call readers' attention to the fact that there are severe difficulties with the accurate determination of the universality class at the temperatures approaching the tricritical point, due to particularly large corrections to scaling associated with the crossover from one universality class to another. The inset to Fig. 27, which shows the cumulants versus chemical potential at $T=0.8$ (i.e., well above T_{trc}) obtained for different sizes of the simulation cell, illustrates this problem. Namely, it is quite well seen that the cumulants obtained for $L=40$, 60, and 80 seem to intersect at the point of U^* equal to about 0.597. When, however, a still larger system of $L=100$ is used the intersection point moves up to the value of about 0.612, i.e., very close to the expected value characteristic to the 2D Ising universality class. At still lower temperature equal to 0.75, we have not reached the scaling regime even with $L=100$, as Fig. 27 shows. Of course, we would finally obtain the proper (Ising) value of U^* if still larger simulation cells were used. We have not performed such calculations, which would require an unreasonably large investment of computer resources, since it is rather obvious to what result would we arrive at. The critical exponents γ and ν along the critical line have been estimated from the finite size scaling analysis, and the results obtained at the temperatures above 0.8 are consistent with the Ising universality class. On the other hand, the critical exponents at the tricritical point are expected to be different, and equal to $\nu=5/9$ and $\beta=1/24$.[62,63,65,66]

When Δu_2 increases to zero and then further to positive values the topology of the phase diagram changes again. It is caused by the decrease of the temperature of the order-disorder transition of the *AF* phase. Table V gives the locations of this transition (T_o^*) at the density equal to unity. Thus, when Δu_2 becomes sufficiently large the temperature T_o^* is lower than the critical temperature of the $c(2\times2)_F$ to the high-density phase transition. In such situation the order-disorder transition of the *AF* phase starts at the critical endpoint (CEP) located at the high-density branch of the coexistence curve of the transition from low- to high-density

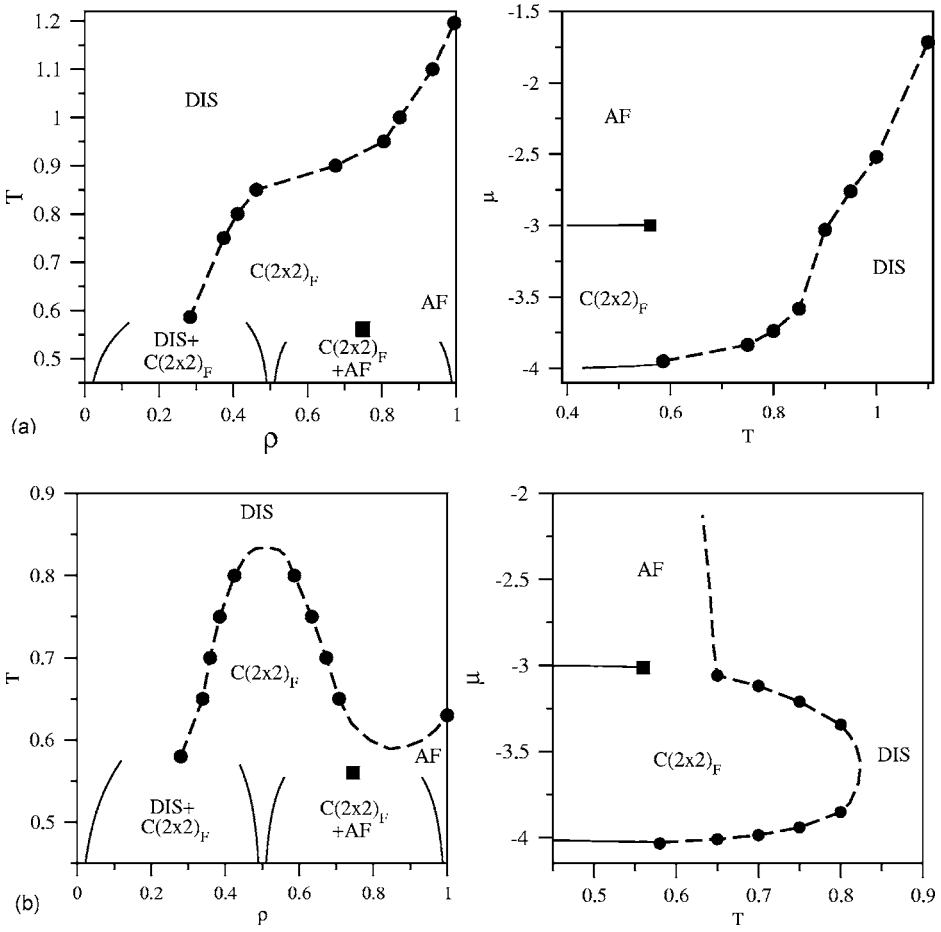

FIG. 26. The density-temperature phase diagrams for the systems with $\Delta u_1=0.5$ and $\Delta u_2=-0.5$ (a) and -0.1 (b).

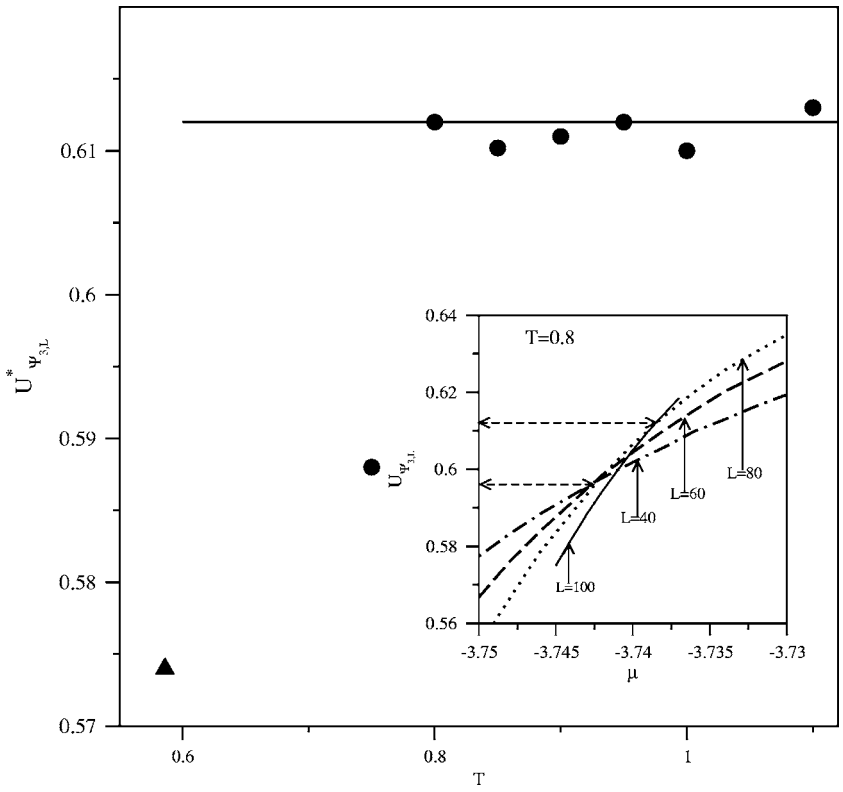

FIG. 27. The changes of the order parameter cumulant fixed-point value at the line of continuous order-disorder transition for the phase $c(2\times2)_F$ (filled circles) and at the tricritical point (filled triangle), for the system with $\Delta u_1=0.5$ and $\Delta u_2=-0.5$. The largest error is equal to ±0.002. The inset shows the changes of the cumulants with μ at the temperature $T=0.8$, obtained for different sizes of the simulation cell (shown in the figure).

TABLE V. The temperatures of the order-disorder transition, T_o, for the phase AF at the density $\rho=1$.

Δu_2	T_o
0.25	0.000
0.23	0.044
0.20	0.110
0.10	0.304
0.00	0.470
−0.10	0.630
−0.50	1.197

phase. Of course, when Δu_2 approaches the threshold value equal to 0.25, the temperature of that order-disorder transition ultimately reaches zero. As a consequence of that downward shift of the order-disorder transition temperature, the line of critical points, starting at the tricritical point, which terminates the gas-$c(2\times2)_F$ transition (at the density 0.25), does not extend to the density equal to unity, but ends at lower density, equal to about 0.75, at the second tricritical point, which replaces the critical point of the transition from the $c(2\times2)_F$ structure to a dense phase. The above statements are supported by the density and the order parameter distributions calculated in a close vicinity of the tricritical point and the critical points of the transition between the $c(2\times2)_F$ and *AF* phases, for the systems characterized by $\Delta u_1=0.5$ and two different values of Δu_2 equal to 0.0 [Fig. 28(a)] and −0.1 [Fig. 28(b)]. In both cases the density distributions demonstrate that we are still in the two-phase region, while the respective order parameter distributions are quite different. When $\Delta u_2=0.0$ we observe three maxima. The maximum located at $\Psi_1=0$ is due to the disordered phase, while two other maxima, at about ±0.32 are due to differently oriented *AF* phases. On the other hand, the order parameter distribution obtained for the system with $\Delta u_2=-0.1$ possesses two maxima only. The maximum at $\Psi_3\approx-0.5$ is associated with the $c(2\times2)_F$ structure, frozen in one of the two possible degenerated states, while the second maximum, at $\Psi_3\approx-0.75$, is due to the *AF* phase, also frozen in one of the two possible degenerated states. Of course, when the two ordered states are locked in other orientations, one obtains the order parameter distributions with only positive values of the order parameter, with the maxima located at Ψ_3 equal to about 0.5 and 0.75, respectively.

VI. CONCLUSIONS

In this work we have presented the results of an extensive Monte Carlo study of the extended BEG spin-1 model with the first- and the second-nearest neighbor interactions. The results presented in this work demonstrate that the lattice gas model discussed exhibits a rich variety of ordered structures of different symmetry and has a quite complex phase behavior. In particular, the phases *AF*, *SAF*, and A_3B have been found to undergo continuous order-disorder phase transitions at the temperatures well below the critical point. It has been shown that the phase transitions associated with the disordering of the phases A_3B and *SAF* are nonuniversal and the critical exponents strongly depend on the model parameters. In the case of nonrepulsive first-nearest neighbor interactions we have not discussed in detail the properties of the model near the critical points of the transition from the gas to the condensed phase. In particular, we have neglected the question to what universality class this transition belongs when the low-temperature ordered structure corresponds to either the *SAF* or A_3B phase.

Then, assuming that the first-nearest neighbor interactions are nonattractive, we have investigated the changes of the phase diagram topology with the magnitudes of the coupling constants. In particular, we have assumed that the surface field leads to a preferential orientation of the molecules with the spin variable $S_i=1$. Under such conditions the ground state analysis predicts the formation of two different ordered states of the density $\rho=0.5$, which correspond to the $c(2\times2)$ ferro- and antiferromagnetic structures, and four different ordered structures (ferro, antiferro, A_3B, and superantiferro) of the density $\rho=1$. With the assumed values of the coupling constants we have excluded from the discussion the phase A_3B.

The results obtained have demonstrated that the topology of the phase diagram changes when different types of order-

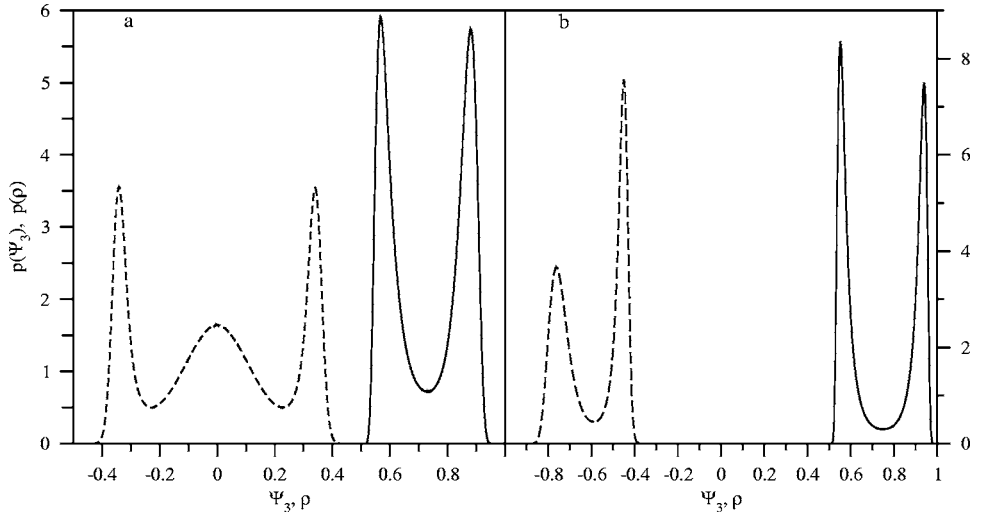

FIG. 28. Distributions of the order parameter Ψ_3 (dashed lines) and of the density (solid lines) for the systems with $\Delta u_1=0.5$ and two different vales of Δu_2 equal to 0.0 at $T=0.604$ and $\mu=-3.096$ (a) and $\Delta u_2=-0.1$ at $T=0.559$ and $\mu=-3.011$.

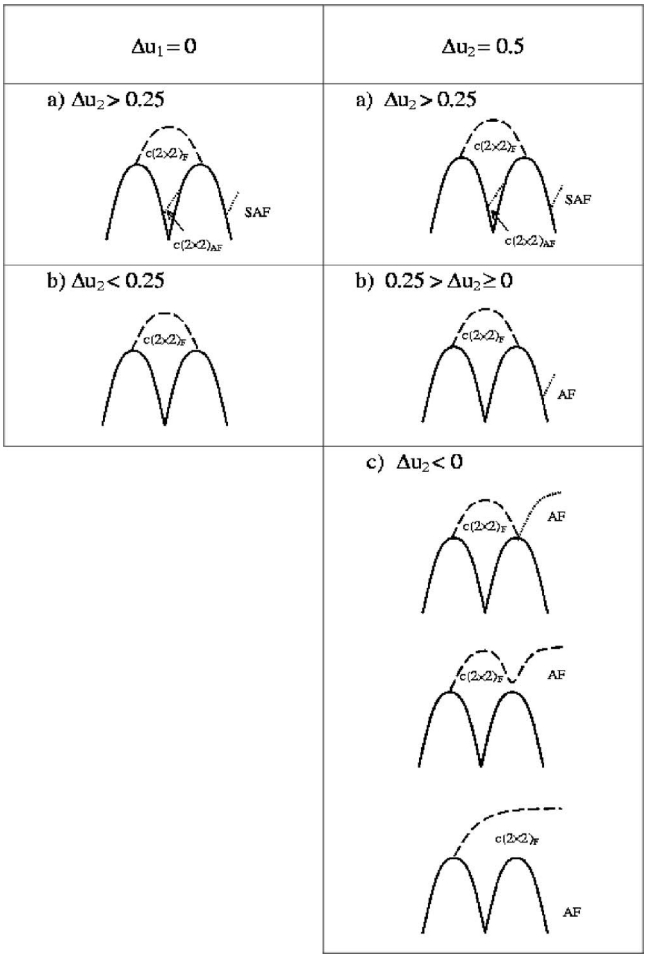

FIG. 29. Schematic representation of the phase diagram topologies for the systems with different values of Δu_1 and Δu_2. Solid lines represent the first-order transitions, while the dashed and dotted lines correspond to continuous transitions.

ing occur in the system. In the case when $\Delta u_1 = 0.0$ we have found two different topologies of the phase diagram, depicted in the left panels of Fig. 29, depending on the magnitude of Δu_2. On the other hand, when $\Delta u_1 = 0.5$ four different topologies appear (see the right panels of Fig. 29) depending, again, on the magnitude of Δu_2. The lower panel on the right-hand side of Fig. 29 shows three different phase diagrams predicted to occur for $\Delta u_2 < 0$. One should note that only two of them have been found in this work (cf. Fig. 26). The appearance of the third phase diagram, which exhibits the presence of multicritical point at the density $\rho = 0.75$, can be anticipated from the fact that the onset of the order-disorder transition of the AF phase, located at the coexistence curve between the $c(2\times2)_F$ and the AF phases at the critical end point $T_{e,2}$, moves towards higher temperatures when Δu_2 decreases. Thus, for a certain value of Δu_2 it has to reach the temperature of the tricritical point. Upon further decrease of Δu_2, the multicritical point disappears and is replaced by a critical point. When it happens, there exists a certain temperature range over which the low-density phase $c(2\times2)$ transforms into the dense AF phase gradually, and not via a phase transition of any type. The phase diagrams exhibiting the presence of such a multicritical point is expected to be found whenever the values of the parameters Δu_1 and Δu_2 are chosen in such a way that the critical end point $T_{e,2}$ coincides with the tricritical point temperature.

One of rather unexpected results has been the finding of the transitions between the $c(2\times2)_{AF}$ and $c(2\times2)_F$ ordered structures, as well as between the *SAF* and *AF* ordered structures at finite temperatures, when the ground state analysis predicts that the $c(2\times2)_{AF}$ and *SAF* phases are stable at zero temperature.

It has been shown that the simple model presented in this paper exhibits a remarkable richness of critical behavior, and it is hoped that our work will stimulate the search for experimental realizations of such systems.

ACKNOWLEDGMENTS

W. R. acknowledges the support from the Alexander von Humboldt Foundation. This project has been also supported by European Community, under the grant MTKD-CT-2004-509249.

*E-mail: wojtek@cool.umcs.lublin.pl

[1] A. Patrykiejew and S. Sokolowski, Adv. Colloid Interface Sci. **30**, 203 (1989).
[2] W. A. Steele, Chem. Rev. (Washington, D.C.) **93**, 2355 (1993).
[3] E. Umback and H. J. Freund, eds., *Adsorption on Ordered Surfaces of Ionic Solids and Thin Films* (Springer, Berlin, 1993).
[4] W. Rzysko and M. Borowko, Surf. Sci. **520**, 151 (2002).
[5] W. Rzysko and M. Borowko, J. Chem. Phys. **117**, 4526 (2002).
[6] A. Patrykiejew, S. Sokolowski, and K. Binder, Surf. Sci. Rep. **37**, 207 (2000).
[7] N. T. Vu, A. Jaklian, and D. B. Jack, J. Chem. Phys. **106**, 2551 (1997).
[8] D. Schmicker, J. P. Toennies, R. Vollmer, and H. Weiss, J. Chem. Phys. **95**, 9412 (1991).
[9] C. Minot, M. A. Van Hove, and J. P. Biberian, Surf. Sci. **346**, 283 (1996).
[10] J. S. Francisco and M. M. Maricq, Acc. Chem. Res. **29**, 391 (1996).
[11] J. S. Francisco, J. Phys. Chem. **98**, 5650 (1994).
[12] J. S. Francisco, J. Chem. Phys. **105**, 3338 (1996).
[13] T. S. Lee, C. M. Rohlfing, and J. E. Rice, J. Chem. Phys. **97**, 6593 (1992).
[14] J. Sivardiere and J. Lajzerowicz, Phys. Rev. A **11**, 2090 (1975).
[15] M. J. Yeomans, *Statistical Mechanisc of Phase Transitions* (Oxford University Press, Oxford, 1992).
[16] M. Blume, V. J. Emery, and R. B. Griffiths, Phys. Rev. A **4**, 1071 (1971).
[17] J. R. Klein and M. W. Cole, Surf. Sci. **134**, 722 (1983).
[18] J. Sivardiere and J. Lajzerowicz, Phys. Rev. A **11**, 2079 (1975).
[19] J. Sivardiere, *in Proceedings of the International Conference on*

Static Critical Phenomena and Inhomogeneous Sysyems, Karpacz, 1984, Lecture Notes in Physics, Vol. 206 (Springer, Berlin, 1984).
[20] H. H. Chen and P. M. Levy, Phys. Rev. B **7**, 4267 (1973).
[21] K. E. Newman and J. D. Dow, Phys. Rev. B **27**, 7495 (1983).
[22] M. Schick and W. H. Shih, Phys. Rev. B **34**, 1797 (1986).
[23] L. Bahmad, A. Benyoussef, and H. Ez-Zahraouy, Surf. Sci. **552**, 1 (2004).
[24] T. E. Burns and J. R. Dennison, Surf. Sci. **395**, 46 (1998).
[25] T. E. Burns, J. R. Dennison, and J. Kite, Surf. Sci. **554**, 211 (2004).
[26] M. Blume, Phys. Rev. **141**, 517 (1966).
[27] H. W. Capel, Physica (Amsterdam) **32**, 966 (1966).
[28] D. Mukamel and M. Blume, Phys. Rev. A **10**, 610 (1974).
[29] J. W. Tacker, J. Magn. Magn. Mater. **71**, 27 (1987).
[30] C. Buzano and A. Polizzola, Physica A **195**, 197 (1983).
[31] C. Ekiz and M. Keskin, Phys. Rev. B **66**, 054105 (2002).
[32] P. D. Beale, Phys. Rev. B **33**, 1717 (1986).
[33] M. Badehdad, S. Bekhechi, A. Benyoussef, and M. Tonzani, Eur. Phys. J. B **4**, 431 (1998).
[34] D. M. Saul, M. Wortis, and D. Stauffer, Phys. Rev. B **9**, 4964 (1974).
[35] A. N. Berker and M. Wortis, Phys. Rev. B **14**, 4946 (1976).
[36] S. M. de Oliveria, P. M. C. de Oliveria, and F. C. de Sa Barreto, J. Stat. Phys. **78**, 1619 (1995).
[37] A. K. Jain and D. P. Landau, Phys. Rev. B **22**, 445 (1980).
[38] O. F. de Alcantara Bonfim and C. H. Obcemea, Z. Phys. B: Condens. Matter **64**, 469 (1986).
[39] N. B. Wilding and P. Nielaba, Phys. Rev. E **53**, 926 (1996).
[40] S. E. Savel'ev and G. Ramirez-Santiago, Phys. Rev. B **63**, 054424 (2000).
[41] C. Buzano, L. R. Evangelista, and A. Pelizzola, Phys. Rev. B **53**, 15063 (1996).
[42] A. Sigueria and I. P. Fittipoldi, Physica A **138**, 592 (1986).
[43] T. J. Kaneyoshi, Physica C **19**, L557 (1986).
[44] T. J. Kaneyoshi, Physica A **182**, 436 (1992).
[45] B. J. Arora and D. P. Landau, Bull. Am. Phys. Soc. **17**, 300 (1972).
[46] M. Takama and K. Takahachi, Phys. Status Solidi B **93**, L85 (1979).
[47] A. Bobak, S. Moscovciak, M. Jurcisin, and M. Jascur, Physica A **230**, 703 (1996).
[48] W. Hoston and A. N. Berker, Phys. Rev. Lett. **67**, 1027 (1991).
[49] M. P. Allen and D. J. Tildesley, *Computer Simulation of Liquids* (Clarendon Press, Oxford, 1987).
[50] D. P. Landau and K. Binder, *A Guide to Monte Carlo Simulation in Statistical Physics* (Cambridge University Press, Cambridge, 2000).
[51] D. Loison and P. Simon, Phys. Rev. B **61**, 6114 (2000).
[52] K. Binder, Z. Phys. B: Condens. Matter **43**, 119 (1981).
[53] A. M. Ferrenberg and R. H. Swendsen, Phys. Rev. Lett. **61**, 2635 (1988).
[54] A. M. Ferrenberg, *in Computer Simulation Studies in Condensed Matter Physics III*, edited by D. P. Landau, K. K. Moon, and H. B. Schuttler (Springer, Heidelberg, 1991).
[55] Q. Q. Yan and J. J. de Pablo, J. Chem. Phys. **111**, 9509 (1999).
[56] T. S. Kristof and Liszi, Mol. Phys. **99**, 167 (2001).
[57] K. Binder, *in Computational Methods in Field Theory*, edited by C. B. Lang and H. Gausterer (Spring, Berlin, 1992).
[58] M. Schick, Prog. Surf. Sci. **11**, 245 (1981).
[59] G. Kamieniarz and B. W. J. Blote, J. Phys. A **26**, 201 (1993).
[60] K. Binder and D. Heermann, *Monte Carlo Simulation in Statistical Physics: An Introduction* (Springer, Berlin, 2002).
[61] S. Krinsky and D. Mukamel, Phys. Rev. B **16**, 2313 (1977).
[62] B. Nienhuis, J. Phys. A **15**, 199 (1982).
[63] W. Selke, D. Huse, and D. Kroll, J. Phys. A **17**, 3091 (1984).
[64] K. Binder, Z. Phys. B: Condens. Matter **43**, 119 (1981).
[65] D. B. Balbao and J. R. Druchowich de Felicio, J. Phys. A **20**, L207 (1987).
[66] D. Friedan, Z. Qiu, and S. Shenker, Phys. Rev. Lett. **52**, 1575 (1984).